

Strain rates at high temporal resolution from curved inclusion trails in garnet, Passo del Sole, Central Swiss Alps

C. A. BERG,* W. D. CARLSON AND J. N. CONNELLY†

¹Department of Geological Sciences, The University of Texas at Austin, Austin, TX 78712, USA (cberg@westga.edu)

ABSTRACT Quantitative strain rates at outcrop scale are very difficult to obtain, but they may be estimated from crystals with curved inclusion trails by calculating rotation rates from growth rates and corresponding deflections of the internal foliation. Garnet in a quartzose pelite at Passo del Sole in the central Swiss Alps is extraordinarily valuable for calculation of strain rates during Alpine orogenesis, because the unusual zoning patterns clearly define the kinetics of its nucleation and growth. Complex concentric zoning patterns can be correlated from one crystal to another in a hand sample, based on compositional and microstructural similarities; the ubiquity of these features demonstrates that all garnet crystals nucleated at nearly the same time. Compositional bands whose radial widths are proportional to crystal size provide evidence for growth governed by the kinetics of intergranular diffusion of locally sourced nutrients. Together, these constraints increase the reliability of estimates of rates of garnet growth, and the strain-rate calculations that depend on them. To obtain growth rates, *P*–*T* conditions during garnet crystallization were modelled in a series of pseudosections, and compositional evolution was connected to rates of garnet growth by means of an independently determined heating rate. These growth rates, combined with measured amounts of curvature of inclusion trails, indicate that the time-averaged strain rate at Passo del Sole during Alpine metamorphism was on the order of 10^{-14} s⁻¹. Strain rates calculated using rotational v. non-rotational models are similar in magnitude. The constraints on crystallization kinetics also allow direct calculation of strain rates during individual stages of garnet growth, revealing short-term increases to values on the order of 10^{-13} s⁻¹. These higher strain rates are correlated with the growth of concentric high-Ca or high-Mn zones in garnet, which implies that strain softening associated with the transient passage of fluids is responsible for acceleration of deformation during these intervals.

Key words: Alpine metamorphism, garnet, Lepontine Dome, strain rate, strain softening.

INTRODUCTION

Strain rate is a quantifiable descriptor of the evolution of rock textures and of deformation during metamorphism. For example, data on rates of shear strain can aid the interpretation of inclusion fabrics in metamorphic rocks, constraining the timing of fabric formation or deformational systematics (Barker, 1994). Strain-rate data have also been used to evaluate the emplacement rates of intrusive bodies within their host rocks by providing a means to estimate the rate at which wall rocks deformed to create accommodation space for an expanding plutonic body (e.g. Paterson & Tobisch, 1992).

Other agents of metamorphism, such as pressure, temperature, composition of mineral or fluid phases and time, are commonly evaluated by well-established petrological and geochronological techniques. By

comparison, few strain-rate data exist for prograde metamorphic rocks. Some of the strain-rate calculations listed in Table 1 represent orogen-scale measurements (Pfiffner & Ramsay, 1982; McCaffrey, 1996); these are unlikely to be applicable on the outcrop or hand-specimen scale. Other techniques retrieved strain-rate values on a thin-section scale (e.g. Müller *et al.*, 2000), but are based on microstructural analysis of mica crystals that are prone to dynamic recrystallization processes, which prevents them from preserving the entire deformational history of the rock, especially if peak conditions reached high temperatures. Still other methods relied upon detailed geochronological analysis of cores and rims of porphyroblasts in combination with a textural analysis of their inclusion patterns (Christensen *et al.*, 1989, 1994; Vance & O'Nions, 1992; Baxter & DePaolo, 2004); these methods, while potentially quite accurate, are time and resource intensive, and require relatively large porphyroblasts. Biermeier & Stüwe (2003) pioneered a promising new method of strain-rate estimation that pairs textural analysis of inclusion trails within porphyroblasts with thermodynamic models of garnet growth; we adapt and extend their approach in this study.

*Present address: Department of Geosciences, University of West Georgia, Carrollton, GA 30118, USA

†Present address: Center for Star and Planet Formation, Natural History Museum of Denmark, University of Copenhagen, Øster Voldgade 5-7, Copenhagen DK-1350, Denmark

Table 1. Previous strain-rate measurements.

Method	Strain rate (s^{-1})	Authors
Garnet rotation/growth rates	6.6×10^{-14}	Biermeier & Stüwe (2003)
Garnet rotation/Gibbs model	$5\text{--}10 \times 10^{-13}$	Holm & Selverstone (1990)
Garnet rotation/assumed growth rate	$2.5\text{--}7.3 \times 10^{-14}$	Baxter & DePaolo (2004)
Rb–Sr strain fringes	$1.1\text{--}7.7 \times 10^{-15}$	Müller <i>et al.</i> (2000)
Rb–Sr garnet growth zones	2.7×10^{-14}	Christensen <i>et al.</i> (1994)
Rb–Sr garnet growth zones	1.9×10^{-14}	Vance & O'Nions (1992)
Rb–Sr garnet growth zones	2.4×10^{-14}	Christensen <i>et al.</i> (1989)
Arc-scale: seafloor-spreading rates	$1\text{--}100 \times 10^{-15}$	Pfiffner & Ramsay (1982)
Arc-scale: earthquake slip vectors	$0.3\text{--}3.2 \times 10^{-15}$	McCaffrey (1996)

For several reasons, garnet has become the principal target mineral for assessing outcrop-scale strain rates during dynamothermal metamorphism. Garnet is a common porphyroblastic phase in most rocks of pelitic bulk composition at or above upper greenschist facies conditions. Rates of intracrystalline diffusion of major components in garnet are relatively slow compared with other common pelitic phases, so garnet can preserve a detailed record of compositional variation as a function of P – T during prograde growth. Garnet crystals typically are not recrystallized or dissolved in response to deformational processes, especially relative to other pelitic phases such as biotite. Finally, the commonly equant habit of garnet crystals is ideally suited for strain-rate analysis, because crystals growing in a deforming matrix may be modelled as spheres, removing the influences of crystallographic orientation and dimensional anisotropy with respect to deformation, and decreasing the complexity of numerical simulations that attempt to replicate observed internal fabrics in natural samples (e.g. Rosenfeld, 1970; Schoeneveld, 1977; Masuda & Mochizuki, 1989). In contrast, inequant porphyroblasts, such as staurolite, exhibit more complex behaviours during syn-deformational growth that are influenced by the crystals' original orientations with respect to the direction of shear (e.g. Biermeier *et al.*, 2001; Busa & Gray, 2005).

These physical and chemical properties of garnet were used to full advantage by Biermeier & Stüwe (2003) to produce strain-rate estimates for garnet-bearing samples from the Tauern Window, Austria. Their method combines two separate measurements: (i) a calculation of the volume of garnet growth during an individual time step, using assumed heating rates along the prograde P – T – t path, based on thermodynamic models that use bulk compositional data to assess stable assemblages and mineral compositions; and (ii) a determination of the total amount of core-to-rim curvature of quartz inclusion trails contained within the porphyroblast. These two measurements, when combined, give a rate of apparent rotation for the garnet, which is half the strain rate if the curvature is the result of rigid-body rotation during growth from a matrix undergoing simple shear (e.g. Rosenfeld, 1970; Williams & Jiang, 1999): thus, $\dot{\omega} = \dot{\gamma}/2$, in which $\dot{\gamma}$ is strain rate and $\dot{\omega}$ is the rotation rate. Although

Biermeier & Stüwe (2003) were successful in their attempts to measure the strain rate averaged over the entire period of garnet growth, they were unable to calculate meaningful strain rates for individual time intervals or growth steps in the garnet growth history, due to uncertainties within their thermodynamic models and difficulty in verifying their assumptions about the nature of garnet nucleation and growth in their specimen. This study refines and re-applies the method developed by Biermeier & Stüwe (2003), using a suite of samples from the Central Swiss Alps whose garnet growth history can be more thoroughly and precisely characterized; it generates not only estimates of time-averaged overall strain rates, but also estimates of incremental strain rates for successive stages in the garnet growth history.

An assumption common to many published strain-rate analyses is that the curved inclusion trails in snowball or spirally included garnet porphyroblasts are formed due to rotation of the porphyroblast within the deforming matrix (Passchier *et al.*, 1992; Williams & Jiang, 1999; Johnson *et al.*, 2006). However, a dissenting viewpoint holds that garnet porphyroblasts remain fixed with respect to geographical coordinates during dynamothermal metamorphism, and the internal textures within a garnet porphyroblast are produced by progressive overgrowth of garnet onto successive generations of matrix foliation surfaces (e.g. Bell, 1985; Bell *et al.*, 1992a,b). Although the methods of calculating strain rates with respect to fabrics within garnet for the rotational and non-rotational cases are dissimilar, strain-rate values may still be calculated from the curvature of inclusion trails if one can determine the amount of shortening associated with the development of a new, orthogonal foliation surface (Johnson & Williams, 1998). This study compares strain-rate estimates for both the rotational and non-rotational models of spiral-inclusion-trail development during prograde garnet growth.

This analysis begins by assessing the advantages of using garnet from Passo del Sole for calculation of strain rates during prograde Alpine metamorphism via re-application of the method developed by Biermeier & Stüwe (2003). Next, Lu–Hf geochronological data are presented to rule out the possibility that these unique zoning patterns resulted from pre-Mesozoic garnet cores rimmed by Alpine overgrowths, rather than from a single Barrovian-style metamorphic event. Thermal models of garnet growth are then constructed via pseudosections, and are combined with heating-rate estimates to yield constraints on the rate of garnet growth in these samples. Finally, these garnet growth rates will be integrated, first with progressive changes in the angle of deflection of inclusion trails in individual garnet crystals in the rotational case, and then with the development of successive orthogonal matrix fabrics in the non-rotational case, to generate estimates of strain rates for individual garnet growth zones.

GEOLOGICAL SETTING

Passo del Sole is located along the Northern Steep Belt of the Lepontine Dome (Frey & Mählmann, 1999), ~75 km southeast of Luzern and 5 km southwest of Lukmanier Pass (Fig. 1a). Alpine structures at this locality are associated with shortening, subduction and back-thrusting of nappes within an accretionary prism, and continent–continent collision in the mid-Tertiary. At least three phases of deformation are preserved along the Northern Steep Belt: tectonic emplacement of nappes, formation of large-scale folds such as the Scopi and Piora synclines and the development of backfolds (Chadwick, 1968; Thakur, 1973). In the Lukmanier region, the Lucomagno nappe was tectonically emplaced over the Mesozoic cover sequence (meta-evaporites, quartzites and mafic schists) of the Gotthard massif (Fig. 1b). The tectonic boundary very nearly coincides with the core of the Piora syncline, and metasedimentary units in the Gotthard cover sequence are thinned, truncated or both on the south limb of the fold. The study area straddles the boundary between the Helvetic zone to the north, where pre-Alpine (Hercynian, *c.* 300 Ma) metamorphic mineral assemblages are overprinted by Alpine metamorphism and deformation, and the interior of the Lepontine Dome to the south, where high-grade metamorphism has completely obliterated and reworked the pre-Alpine

assemblages (Fig. 1; Frey *et al.*, 1980). Metamorphism in this vicinity reached amphibolite facies conditions of 550–600 °C and 6–9 kbar, and peak pressures and temperatures increase rapidly to the south (Todd & Engi, 1997; Frey & Mählmann, 1999; Janots *et al.*, 2009). In the vicinity of Passo del Sole, late-stage backfolding has overturned the sequence so that the overthrust Lucomagno nappe now makes up the footwall of the shear zone (Fig. 1b; Chadwick, 1968).

This study is focused on garnetiferous samples collected from the Orange Gneiss, a rusty-weathering, garnet ± staurolite ± kyanite + biotite + muscovite + plagioclase + quartz pelitic unit that crops out along the northern boundary of the Lucomagno nappe (Fig. 2). Locally, the Orange Gneiss is interlayered with thin (1–2 m thick) discontinuous lenses of amphibolite. In the vicinity of the tectonic boundary, the metamorphic foliation is steeply north-dipping; individual mica-rich or quartz-rich layers are thinned, and early generations of quartz veins are dismembered and boudinaged (Chadwick, 1968). Garnetiferous layers contain porphyroblasts with spiral inclusion fabrics that are visible in outcrop and preserve a south-side-up sense of apparent rotation (Rosenfeld, 1987). These microstructures indicate that the tectonic boundary between the Lucomagno nappe and the metasedimentary cover sequence of the Gotthard massif was active as a shear zone during Lepontine metamorphism.

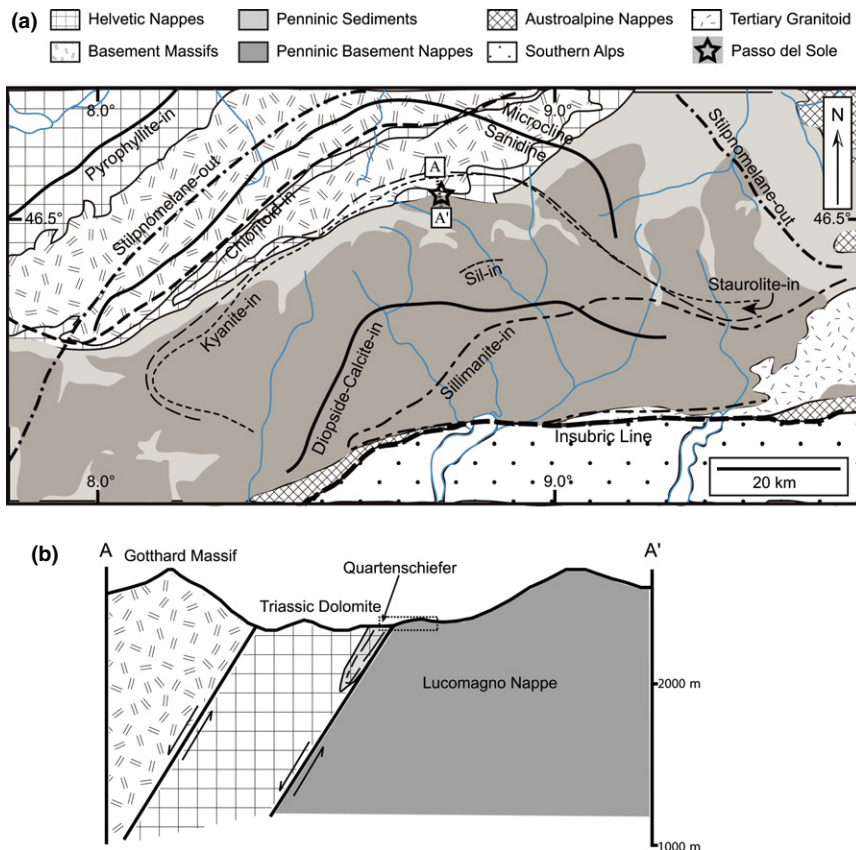


Figure 1. (a) Generalized tectonic map of the Lepontine Dome and the surrounding area showing mineral isograds developed during Alpine metamorphism (after Frey & Mählmann, 1999). Star indicates location of Passo del Sole and study area. (b) Cross-section A-A' in the vicinity of Passo del Sole (after Chadwick, 1968). Arrows indicate direction of shear. See text for further discussion. Dashed rectangle outlines area shown in Fig. 2.

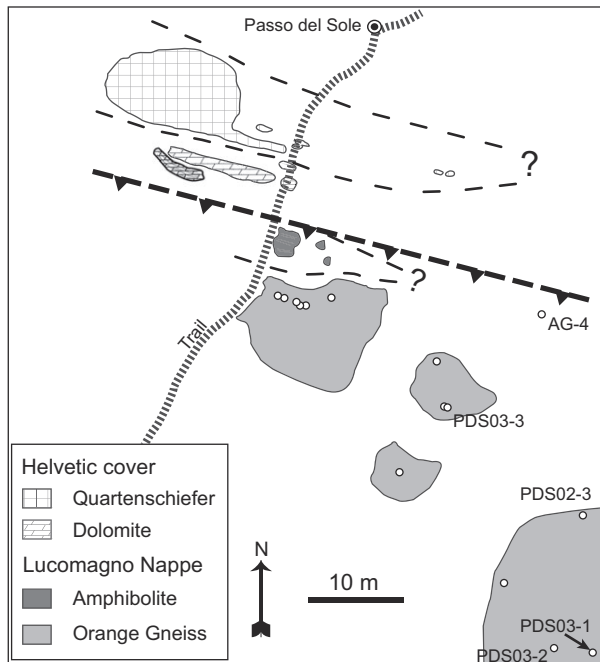


Figure 2. Outcrop map showing local geology at Passo del Sole (Lat.: 46.531997°N; Long.: 8.770895°E). Dashed contacts are not exposed at the surface. Open circles represent sampling locations in the Orange Gneiss; samples described in text are labelled. The outcrop from which AG-4 was collected has since been obliterated.

PREVIOUS WORK: SAMPLE AG-4

The obvious overlap of deformation and metamorphic mineral growth at Passo del Sole led to an attempt by Meth & Carlson (2005) to quantify garnet growth mechanisms active in such an environment. Their observations of garnet textures and chemistry are the basis for selecting this area for further study. The work of Meth & Carlson (2005) was based on a single specimen of Orange Gneiss, sample AG-4, originally collected by J. Rosenfeld, from an outcrop at Passo del Sole very near the shear zone boundary between the tectonic units (Fig. 2). Although the hand sample was unremarkable beyond the well-developed syn-kinematic spiral inclusion trails preserved within garnet, X-ray mapping of the garnet revealed unique and unexpected compositional zoning patterns (Fig. 3), described in detail in Meth & Carlson (2005). All garnet within the hand specimen displays complex, concentric Ca zonation, with multiple oscillations in Ca content producing a pattern akin to tree rings. Especially notable is that these patterns of compositional variation are identical in all garnet crystals, and thus compositions can be correlated among all crystals in the hand sample. For example, at the position of the large Ca spike just outside the garnet core (arrow, Fig. 3), all garnet crystals have near-equal chemical compositions within a very narrow range. This indicates that shortly after the initiation of garnet growth,

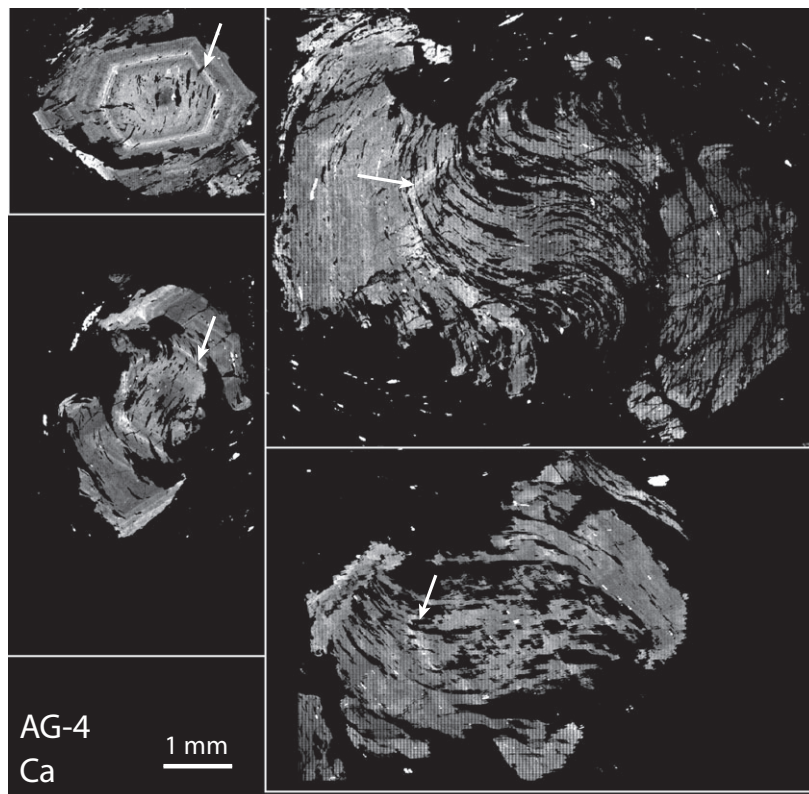


Figure 3. Ca X-ray maps for selected garnet from sample AG-4 (Meth & Carlson, 2005). X-ray maps were made on centred sections oriented perpendicular to the axis of apparent rotation based on HRXCT analysis. Arrows highlight the correlation of high-Ca spikes with the onset of curvature in the quartz inclusion trails.

major-element equilibrium had been achieved on the scale of the hand sample. In addition, the width of each individual compositional zone is proportional to the size of the porphyroblast; small crystals have narrow zones, and large crystals have proportionally wider zones. Meth & Carlson (2005) also observed that the complex Ca-zoning patterns could be correlated between porphyroblasts on a microstructural basis. In each crystal, the position of the Ca spike corresponds to a position in the porphyroblast where the planar quartz-inclusion trails in the core transition to curved inclusion trails in the rim; the amount of angular deflection at the Ca spike is roughly 30°. These compositional and microstructural correlations for porphyroblasts in sample AG-4 have important advantages for efforts to model garnet growth rates, which will be discussed in detail below. Unfortunately, the outcrop from which sample AG-4 was collected in 1963 was obliterated during subsequent construction of a concrete-lined tunnel at the pass, therefore, direct sampling of the layer from which AG-4 was collected is no longer possible.

COMPOSITIONAL VARIATIONS WITHIN GARNET

Methods

A new suite of hand specimens was collected from Passo del Sole and vicinity (Fig. 2). Oriented thin sections were produced, cut orthogonal to the well-developed foliation, parallel to the biotite stretching lineation and orthogonal to the axis of apparent rotation of the garnet porphyroblasts. Reconnaissance X-ray maps of non-centrally sectioned garnet crystals made using a JEOL 8200 electron microprobe at The University of Texas at Austin were used to appraise the characteristics of compositional zoning within garnet, and to facilitate the selection of samples for central sectioning and thermodynamic modelling. Final selection of samples for further study was made on the basis of identification of easily recognizable, texturally and chemically consistent growth-zoning patterns in garnet porphyroblasts.

For samples chosen for detailed analysis, central sections through garnet were located by high-resolution X-ray computed tomography at The University of Texas at Austin (Carlson & Denison, 1992; Denison & Carlson, 1997). Digital reslicing through garnet centres was used to evaluate the orientation of the maximum inclusion curvature with respect to the cut slab; the normals to the cut surfaces were found to be within 5° of the garnet rotation axes, a level of uncertainty that corresponds to <1° of change in the total inclusion curvature as determined from image analysis. Garnet X-ray maps and quantitative EPMA analyses of garnet and other major rock-forming phases were used to characterize the composition of the samples and to document the uniformity of chemical-zoning patterns on the scale of a hand specimen.

Results

Sampling of garnetiferous layers of Orange Gneiss at Passo del Sole has not resulted in the discovery of any garnet crystals with zoning equivalent to sample AG-4. Instead, reconnaissance X-ray map analysis revealed that garnet preserves a stunning variety of compositional zoning patterns that vary from layer to layer, and in some cases vary within layers on a metre scale (Berg, 2007). The zoning pattern evident in most garnet at Passo del Sole (Fig. 4) is characterized as follows: cores feature high Mn, high Y and relatively low Ca; moving rimwards, there is a sharp decrease in Y and steady decrease in Mn, whereas Ca is slightly elevated and commonly exhibits patchy zoning; and high-Ca zones are present as discontinuous rims on many porphyroblasts. Comparison of these analyses has identified a 'baseline' compositional zoning pattern that is interpreted to represent zoning produced by closed-system, prograde regional metamorphism, upon which local perturbations, produced by open-system behaviour, are superimposed. Identification of this regional 'baseline' compositional zoning signature will prove useful when comparing garnet crystals that have been affected by different open-system processes, as described below.

Garnet in sample PDS03-1, from an outcrop ~30 m to the south of the former position of AG-4 (Fig. 2), displays compositional zoning patterns that are dissimilar in style to those seen in AG-4, but equivalent in their ability to show textural and compositional correlations between porphyroblasts on the scale of a hand sample (Fig. 5a). Concentric compositional zoning patterns in sample PDS03-1 contain several notable features. Like sample AG-4, garnet in this sample displays a high-Ca rim. However, it lacks the oscillatory Ca zoning and the large high-Ca spike near the core of the porphyroblast seen in sample AG-4. Instead, the most unusual feature of garnet in sample PDS03-1 is a high-Mn annulus near the rim, just in-board of a sharp increase in Ca content. A Mn annulus of this scale is unique to this sample, among all samples collected at Passo del Sole. Like the Ca-zoning features described earlier, this concentric Mn zone can be correlated texturally and chemically throughout the specimen.

The origin of this broad Mn annulus must be addressed before this sample may be used for garnet growth-rate-modelling calculations. Although this zoning feature is present in all garnet crystals analysed in sample PDS03-1, another sample (PDS03-2) collected from the same garnetiferous layer only 5 m east along strike from PDS03-1 completely lacks the Mn annulus. In fact, garnet crystals from this neighbouring sample display an entirely different set of concentric zoning patterns in Ca and Mn (Fig. 5c). Because the layer is lithologically homogeneous, the two samples are mineralogically identical, which makes it unlikely that the Mn annulus in PDS03-1 formed as the result

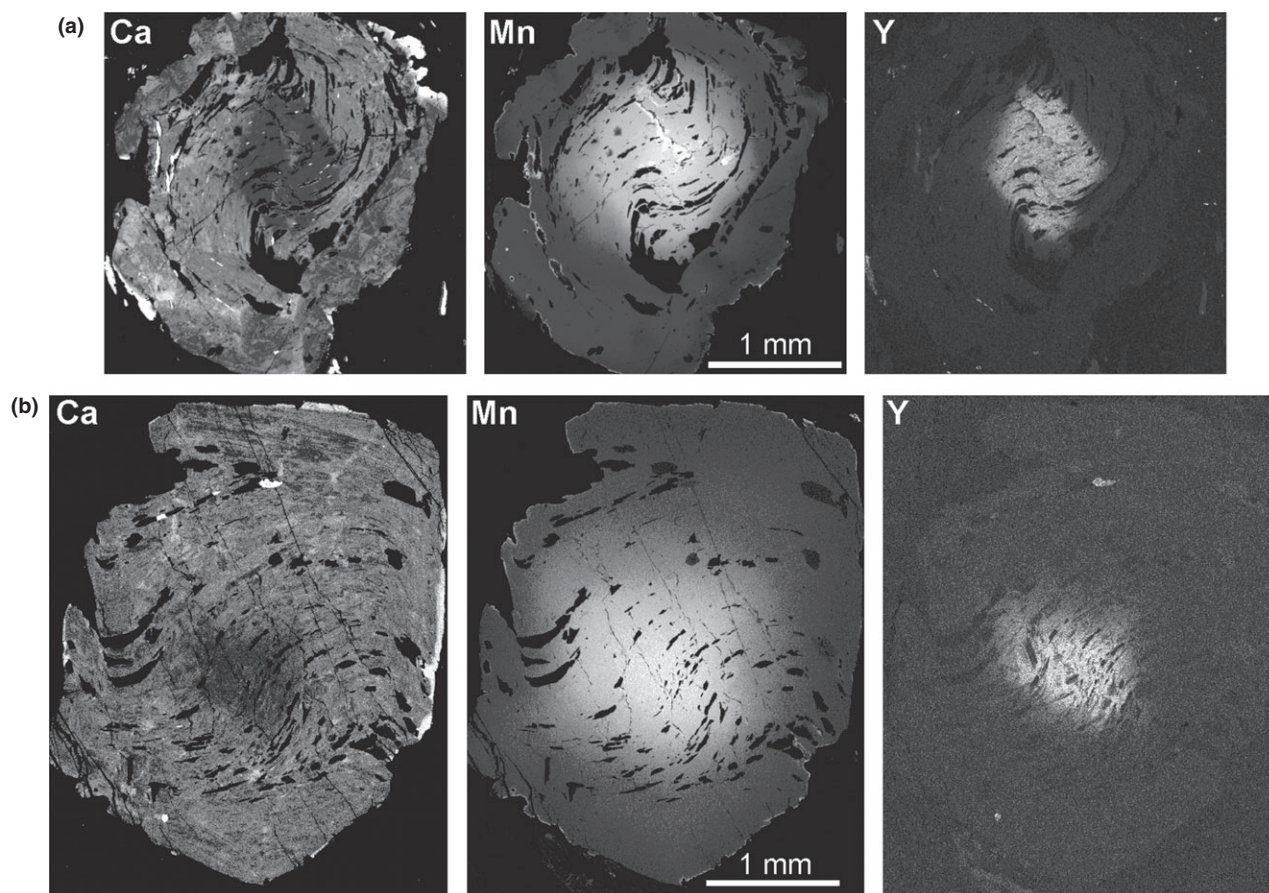


Figure 4. Ca, Mn and Y X-ray maps for garnet from (a) PDS02-3 and (b) PDS03-3, which show typical 'baseline' zoning patterns upon which the unusual Ca- or Mn-zoning patterns found in samples AG-4 and PDS03-1 are superimposed. Typical zoning patterns include bell-shaped Mn-zoning profiles, low-Ca and high-Y cores, near-rim patchy Ca zoning and high-Ca rims. See text for further discussion.

of the breakdown of a Mn-rich phase within the pelitic layer, a mechanism that has been hypothesized to produce Mn annuli in other settings (Yang & Rivers, 2001, 2002). A plausible alternative is that the Mn annulus, and similar local variations in Ca and other cations in garnet, are the result of transient, channelized fluid flow in pathways localized along the shear zone boundary. This hypothesis will be explored further later in this article. A third possibility is that the Mn zoning is the result of two distinct episodes of metamorphism, separated by an interval of resorption of garnet. If this hypothesis is correct, it raises concerns for the applicability of garnet-growth modelling to samples from Passo del Sole: if garnet cores nucleated and grew during a pre-Alpine metamorphic event, growth-rate models that assume that all garnet crystallization occurred during a single orogenic pulse would overestimate rates of garnet growth. Textural evidence, such as the internal fabrics preserved within garnet, might be interpreted to support this hypothesis: garnet cores contain planar inclusion trails, indicating that the early history of garnet growth occurred in the absence of rotation or a reorientation of external fabrics; it is conceivable that the cores of these garnet

crystals grew in a pre-Alpine event. Lu–Hf geochronology was employed to assess the possibility of pre-Alpine core growth.

GEOCHRONOLOGY

Lu–Hf garnet geochronology is a relatively new technique that has been developed to constrain the ages of metamorphism in garnet-bearing assemblages (e.g. Johnson *et al.*, 1996; Scherer *et al.*, 2000; Lapen *et al.*, 2003, 2007; Connelly, 2006). Lu is strongly partitioned into garnet during growth and thus becomes concentrated in the cores of the developing porphyroblasts, so Lu–Hf dating of bulk garnet separates will be strongly weighted towards the age of formation of garnet cores. Consequently, if garnet cores represent a pre-Alpine (Hercynian) crystallization episode, this should be apparent in bulk Lu–Hf ages.

Lu–Hf geochronology was performed on sample PDS03-3, a pelitic sample of Orange Gneiss taken from ~10 m northwest of PDS03-1 (Fig. 2) that exhibited Y zoning patterns and a high-Ca rim zone in garnet similar to those found in samples AG-4 and PDS03-1. These zoning patterns most closely resemble the out-

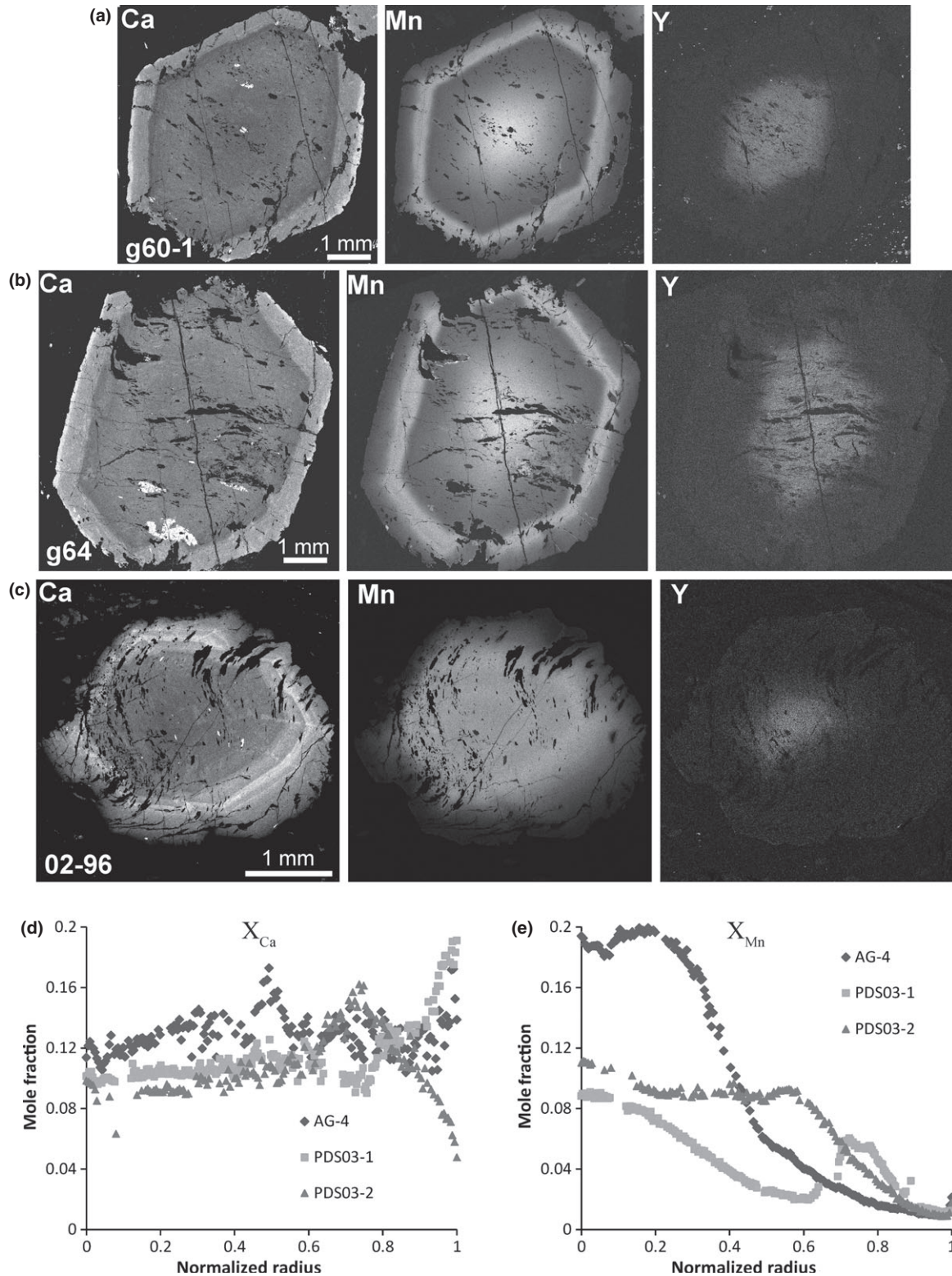


Figure 5. Ca, Mn and Y X-ray maps of garnet from sample PDS03-1 garnet 60-1 (a) and garnet 64 (b); and from sample PDS03-2 garnet 96 (c), which came from the same lithological layer only 5 m distant along strike. Such striking variations in zoning patterns are widespread in garnet samples collected over small areas at Passo del Sole (compare Ca maps to AG-4, Fig. 3). (d–e) Radius-normalized core-to-rim traverse data showing variations in Ca and Mn concentrations in AG-4, PDS03-1 and PDS03-2.

Table 2. Lu–Hf geochronology data for sample PDS03-3.

	Weight (g)	ppm Lu	ppm Hf	$^{176}\text{Lu}/^{177}\text{Hf}$	2 σ % error ^a	$^{176}\text{Hf}/^{177}\text{Hf}$	2 σ % error ^a
Rutile	0.0050	0.1070	11.6752	0.001301	0.58	0.282252	0.011
Garnet 1	0.0580	8.3529	0.1345	8.817280	0.58	0.286449	0.019
Garnet 2	0.0693	6.3338	0.0925	9.719555	0.58	0.286854	0.022

^aErrors based on the external reproducibility of BCR-2 analysed in this period and reported in Connelly (2006).

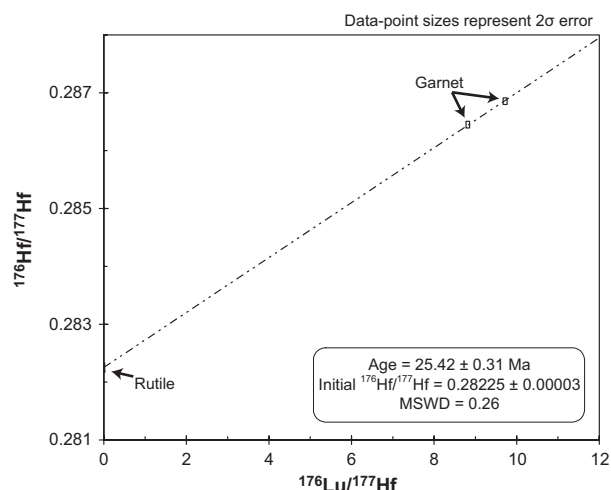


Figure 6. Lu–Hf garnet–rutile isochron for sample PDS03-3. The two measurements on garnet represent duplicate aliquots from the same mineral separate. This age, which is weighted towards the age of the garnet core, rules out the presence of a significant c. 300 Ma (Hercynian) component in the garnet.

crop-scale ‘baseline’ described earlier, upon which local variances in Ca or Mn zoning (e.g. oscillatory zoning or annuli) in other samples are superimposed. The hand specimen was crushed, processed with heavy-liquid and magnetic-separation techniques and hand-picked to produce two 50 mg garnet separates and a 10 mg rutile separate. Each mineral fragment included in these separates was visually inspected for purity based on the lack of inclusions or chemical alteration. To avoid contamination of the Hf measurements for garnet due to microscopic inclusions of zircon, which may contain up to 1.0 w % HfO₂, garnet separates were heat treated to anneal metamict zircon inclusions prior to dissolution, following the procedure described in Connelly (2006). Rutile readily incorporates HFSEs into its structure, but contains little or no Lu; thus, garnet–rutile Lu–Hf isochrons produce the most precise ages possible for these rocks due to their spread in Lu–Hf ratios. Purification and analyses of Lu and Hf followed techniques described by Connelly (2006). Lu and Hf results for basaltic rock standard BCR-2 that were produced during the same period by the same methods employed in this study are also reported in Connelly (2006).

Lu–Hf garnet–rutile analysis for sample PDS03-3 (Table 2) produces a well-constrained isochron age of 25.42 ± 0.31 Ma (Fig. 6), consistent with the timing deduced from allanite and monazite dating by Janots

et al. (2009), who assign porphyroblast growth in this region to the intervals between 29.2 and 31.5, and 18.0 and 19.1 Ma. No evidence is seen of a Hercynian component of garnet growth preserved in the cores of the porphyroblasts. The garnet at Passo del Sole could have nucleated and grown only during the Alpine dynamothermal metamorphism, a conclusion that greatly simplifies growth-rate models and the strain-rate calculations derived from them.

MODELLING GARNET GROWTH

Assumptions required by the model of Biermeier & Stüwe (2003)

The approach taken by Biermeier & Stüwe (2003) to determine garnet growth rates and to calculate strain rates required four separate assumptions about the characteristics of garnet growth and thermal evolution during metamorphism. First, it was assumed that the prograde thermal history evolved with a constant heating rate, which, combined with the modelled thermal evolution of garnet growth, provides the relative timing of porphyroblast growth. Second, it was assumed that the garnet crystals rotated, instead of the alternate model in which internal fabrics result from progressive growth of garnet over successive matrix foliations. Third, it was assumed that the garnet growth rates followed either a constant volumetric growth law or a constant radial growth law. These two rate laws essentially serve as end-members that encompass heat flow-controlled growth processes (constant volumetric growth rate), diffusion-controlled growth processes (constant surface area growth rate) and interface-controlled growth processes (constant radial growth rate). The authors did not determine which of these possible processes governing garnet growth rates was dominant in their sample. Fourth, it was assumed that the timing of garnet nucleation correlated with the size of the garnet in the sample: large crystals were presumed to have nucleated first and small crystals to have nucleated later.

Evaluation of assumptions, Passo del Sole

Although the assumptions made by Biermeier & Stüwe (2003) may well be valid, they are all difficult to verify, and each assumption introduces the potential for errors in the model and adds to the uncertainty of the result. In this study, the number of unverified assumptions required for these calculations was re-

duced. Both studies rely on the assumption that heating rates during metamorphism are constant. However, the prior determination of garnet growth mechanisms at Passo del Sole, in conjunction with careful characterization of the core-to-rim concentric zoning patterns, is a distinct advantage that provides constraints on garnet growth rate and timing of porphyroblast growth. Those constraints make unnecessary the assumptions used by Biermeier & Stüwe (2003) to characterize garnet nucleation and growth; they reduce uncertainties significantly; and they allow examination of strain rates incrementally at stages throughout the growth history, producing high temporal resolution.

Analysis of garnet-zoning patterns in sample AG-4 (Meth & Carlson, 2005) allowed identification of several concentric zones within garnet that can be correlated from porphyroblast to porphyroblast (e.g. Fig. 7). The high degree of correlation among garnet crystals throughout the hand sample is evidence for length scales of diffusion and of chemical equilibration on the order of centimetres (except for Mn in some crystals in unusual microstructural settings; cf. Meth & Carlson, p. 175). Examination of the ratio of the width of individual Ca zones to the size of the garnet porphyroblast revealed that zone width is proportional to garnet size (Fig. 3). These observations led to the determination that the garnet growth mechanism for sample AG-4 was diffusion-controlled growth, in which the garnet growth rate was proportional to the local nutrient supply. Similar systematics are observed

in sample PDS03-1 (Fig. 5a): the widths of individual Ca or Mn zones are proportional to the size of the porphyroblast. This eliminates the need to apply an assumed constant-volume or constant-radius rate law to the growth of garnet.

The work by Meth & Carlson (2005) also provides strong constraints on the relative timing of nucleation and growth of garnet. Under the garnet growth mechanism active at Passo del Sole, the size of an individual porphyroblast does not correlate with the timing of nucleation, a relationship assumed by Biermeier & Stüwe (2003) in their study. Rather, in sample AG-4, small crystals nucleated at approximately the same time as the larger crystals within the hand specimen, as evidenced by central Mn content and Ca-zoning patterns, but grew in regions that were nutrient poor, while the larger crystals grew in regions that were nutrient rich. In addition, the zone-boundary correlation and the behaviour of inclusion-trail fabrics show that each zone boundary can be considered a time marker during garnet growth. For example, the high-Ca spike in each garnet formed at the same time, regardless of position within the hand sample. Similar observations characterize sample PDS03-1: the compositional zoning patterns in garnet are also seen to serve as time markers on the basis of zone-boundary correlation and behaviour of inclusion-trail fabrics.

The combination of a strongly heterogeneous distribution of nutrients in the precursor and limited diffusional competition during crystallization (due to the low number density of porphyroblasts) produced

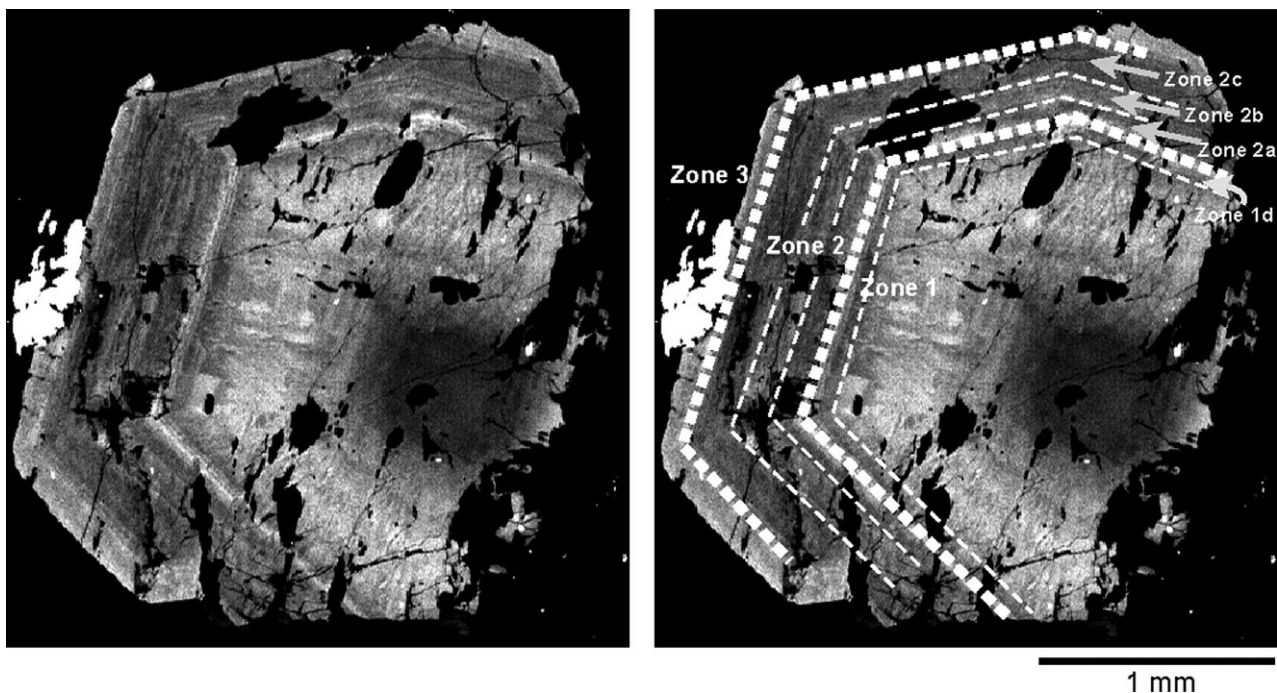


Figure 7. Ca X-ray map of garnet from sample AG-4 (from Meth & Carlson, 2005) showing the concentric zones that were defined on the basis of oscillatory Ca-zoning patterns that can be correlated for each garnet within the hand specimen. The zone boundaries serve as time markers during garnet growth.

size-proportional garnet growth in the rocks of Passo del Sole. In addition, all garnet crystals nucleated nearly simultaneously in the early stages of the crystallization history, probably due to saturation of a limited number of sites favourable to nucleation. The highly fortuitous net result is that all garnet crystals contain, in their compositional zoning patterns, identical and complete records of the progressive prograde increase of garnet mode in the rock as a whole: if a compositional marker (like a high-Ca band) appears after 25 volume per cent of an individual garnet crystal has formed, then one knows that one quarter of the total modal amount of garnet now in the rock had crystallized at the time when that particular compositional marker formed. The distinctive patterns of concentric zoning, when combined with amounts of apparent rotation, therefore reveal changes in strain rate over short intervals of time, and produce a record of extraordinarily high temporal resolution, in addition to the overall time-averaged strain rate during porphyroblast growth.

Garnet growth models

Methods

Thermodynamic modelling of garnet growth was performed using the THERMOCALC v.3.30 software package and accompanying thermodynamic database (Powell & Holland, 1988; Holland & Powell, 1990; Powell *et al.*, 1998). Activity models for pseudosection construction in the chemical system MnNCKFMASH follow the methodology of Tinkham *et al.* (2001) and Stowell *et al.* (2005). Mineral modes were estimated from image analysis of X-ray maps produced from representative thin sections from each sample. The initial bulk com-

position was determined by combining the mineral modes with the compositions (Table 3) and molar volumes of each phase. To take garnet zoning into account in the compositional calculations, the total contribution from garnet in each sample was modelled as a set of nested spheres of different composition.

Pseudosection construction requires the calculation of 'effective' bulk compositions during garnet growth (Stüwe, 1997; Evans, 2004), because components incorporated into the interior of a growing garnet are effectively removed from the system, and matrix phases are unable to interact with them. To accurately model the evolution of the mineralogy and composition of phases within a rock, garnet components must be subtracted from the bulk composition of the rock for each successive interval of garnet growth. Due to the unusual compositional zoning patterns in AG-4 and PDS03-1, one cannot use the procedure of Evans (2004) to estimate garnet modes during growth. Instead, changes in the effective bulk compositions are best modelled in these samples by subdividing garnet growth into segments delimited by compositional zone boundaries, which serve as time markers. For sample AG-4, the garnet growth history is subdivided into five stages defined by the concentric calcium zones (as was done by Meth & Carlson, 2005; cf. Fig. 7):

AG-4 Stage A: from garnet nucleation out to Ca spike.

AG-4 Stage B: from Ca spike out to minor Ca spike (zone 2a/2b boundary).

AG-4 Stage C: zone 2b.

AG-4 Stage D: zone 2c, up to zone 3 boundary.

AG-4 Stage E: discontinuous high-Ca rim.

Concentric zoning patterns were also used to subdivide the growth stages of PDS03-1. However, for this

Table 3. Representative electron microprobe data for mineral compositions.

Sample	Garnet						Staurolite		Biotite		Muscovite			Plagioclase		
	AG-4		PDS03-1		PDS03-2		AG-4	AG-4	PDS03-1	PDS03-2	AG-4	PDS03-1	PDS03-2	AG-4	PDS03-1	PDS03-2
Wt% Ox.	Core	Rim	Core	Rim	Core	Rim	AG-4	AG-4	PDS03-1	PDS03-2	AG-4	PDS03-1	PDS03-2	AG-4	PDS03-1	PDS03-2
SiO ₂	37.60	37.73	36.75	36.94	37.45	37.53	27.40	36.91	37.70	37.33	46.20	46.80	47.15	58.86	61.07	68.33
TiO ₂	0.26	0.03	0.00	0.00	0.00	0.00	0.47	1.31	1.95	1.62	0.39	0.44	0.29	0.00	0.00	0.00
Al ₂ O ₃	20.66	21.28	21.51	21.67	21.41	21.34	53.21	18.71	17.98	19.18	35.96	33.39	33.46	25.01	24.10	19.87
FeO	28.87	32.28	33.37	31.83	32.36	35.03	12.42	15.67	16.85	17.89	1.02	1.28	1.49	0.00	0.00	0.06
MnO	6.12	0.25	3.94	0.52	4.07	0.69	0.16	0.05	0.09	0.04	0.00	0.01	0.00	0.00	0.00	0.00
MgO	1.43	3.72	1.81	3.29	2.24	3.05	1.79	12.60	11.78	11.25	0.66	1.22	1.19	0.00	0.00	0.00
CaO	5.08	4.89	3.57	6.33	3.03	3.36	0.00	0.00	0.02	0.00	0.00	0.00	0.00	6.80	5.61	0.68
Na ₂ O	n.a.	n.a.	n.a.	n.a.	n.a.	n.a.	0.00	0.27	0.19	0.345	1.73	0.56	1.42	8.30	8.28	11.00
K ₂ O	n.a.	n.a.	n.a.	n.a.	n.a.	n.a.	0.00	8.93	9.06	8.43	7.80	10.20	8.74	0.06	0.12	0.04
Total	100.02	100.18	100.95	100.58	100.56	101.01	95.45	94.45	95.62	96.09	93.76	93.90	93.74	99.03	99.18	99.97
Oxygen	12	12	12	12	12	12	46	11	11	11	11	11	11	8	8	8
Si	3.03	3.00	2.95	2.94	3.00	2.99	7.74	2.77	2.79	2.77	3.08	3.15	3.17	2.66	2.73	2.98
Ti	0.02	0.00	0.00	0.00	0.00	0.00	0.10	0.07	0.10	0.09	0.02	0.02	0.02	0.00	0.00	0.00
Al	1.96	1.99	2.04	2.03	2.02	2.00	17.72	1.65	1.62	1.68	2.83	2.65	2.65	1.33	1.27	1.02
Fe ^t	1.94	2.14	2.24	2.12	2.17	2.33	2.94	0.98	1.03	1.11	0.06	0.07	0.08	0.00	0.00	0.00
Mn	0.42	0.02	0.27	0.04	0.28	0.05	0.04	0.00	0.01	0.00	0.00	0.00	0.00	0.00	0.00	0.00
Mg	0.17	0.44	0.22	0.34	0.27	0.36	0.75	1.41	1.32	1.24	0.07	0.12	0.12	0.00	0.00	0.00
Ca	0.44	0.42	0.31	0.54	0.26	0.29	0.00	0.00	0.00	0.00	0.00	0.00	0.00	0.33	0.27	0.03
Na								0.04	0.03	0.05	0.22	0.07	0.19	0.73	0.72	0.93
K								0.85	0.86	0.80	0.66	0.88	0.75	0.00	0.01	0.00

Table 4. Initial and effective bulk compositions (mole per cent oxides) used for thermodynamic modelling.

Growth interval	SiO ₂	Al ₂ O ₃	FeO	MnO	MgO	CaO	Na ₂ O	K ₂ O
AG-4a ^a	69.94	12.98	7.26	0.21	5.03	0.85	0.93	3.10
AG-4b	70.34	13.06	6.54	0.11	5.05	0.72	0.96	3.22
AG-4c	71.20	13.02	5.73	0.06	5.09	0.58	0.99	3.32
AG-4d	71.94	12.99	5.03	0.04	5.12	0.46	1.02	3.40
AG-4e	73.14	12.94	3.90	0.02	5.12	0.28	1.06	3.54
PDS03-1a ^a	64.50	14.76	8.80	0.23	5.38	1.08	0.94	4.31
PDS03-1b	64.89	14.77	8.38	0.21	5.40	1.01	0.96	4.38
PDS03-1c	66.18	14.80	6.96	0.14	5.45	0.80	1.02	4.64
PDS03-1d	67.33	14.83	5.74	0.05	5.49	0.63	1.07	4.87
PDS03-1e	68.31	14.85	4.70	0.01	5.51	0.45	1.11	5.06

^aInitial bulk composition.

sample, the subdivisions include discrete zones identified by Y- and Mn-zoning patterns, as well as variations in Ca content:

PDS03-1 Stage A: garnet nucleation and growth of high-Y core.

PDS03-1 Stage B: from high-Y core out to Mn annulus.

PDS03-1 Stage C: Mn annulus.

PDS03-1 Stage D: region of decreasing Mn content and elevated Ca.

PDS03-1 Stage E: discontinuous high-Ca rim.

Initial bulk compositions and the effective bulk compositions used for successive stages of garnet growth in each sample are compiled in Table 4.

Changes in temperature associated with progressive stages of garnet growth, based on the intersection point of garnet isopleths calculated from electron-microprobe analyses (X_{Ca} , X_{Mn} and $Fe/(Fe + Mg)$) through a series of P - T pseudosections, were combined to determine the thermal evolution during garnet growth. This thermal evolution, combined with estimates of heating rates during Lepontine metamorphism, gives the garnet growth rate.

Oxygen isotope analysis

The unusual compositional zoning used above to define intervals of garnet growth indicates that rocks near Passo del Sole likely experienced influxes of Ca during garnet growth, as in sample AG-4, or influxes of Ca and Mn during garnet growth, as in sample PDS03-1. The large magnitudes and highly variable character of these compositional excursions strongly suggest that they originated via open-system behaviour linked to the passage of fluids capable of modifying local bulk compositions.

That proposed mechanism for producing the observed variations in garnet-zoning patterns can be evaluated by seeking variations in stable isotopic composition in the garnet porphyroblasts. Oxygen isotopic variations associated with the passage of metamorphic fluids have been observed in garnet porphyroblasts in several localities (e.g. Chamberlain & Conrad, 1991; Kohn *et al.*, 1993; Young & Rumble, 1993; Skelton *et al.*, 2002). Concentric zoning in stable

Table 5. Zone definitions for SIMS analysis.

Zone	AG-4	PDS03-1	PDS03-2
1	Garnet core	High Mn core	High Mn core
2	Growth interval 1 Ca spike ^a	Low Mn	First Ca high
3	Growth interval 2a	First Mn high	Second Ca high
4	Growth interval 2b	Mn trough	Third Ca high
5	Growth interval 2c	Ca/Mn rise	Low Ca rim
6	Growth interval 3 (rim)	High Ca zone	
7		Highest Ca (rim)	

^aGrowth intervals as defined by Meth & Carlson (2005).

isotopes has been correlated with major- and minor-element-zoning patterns as time markers for the flow of these fluids through the metamorphic system (Lanzirotti, 1995; Skelton *et al.*, 2002). The development of in situ analytical techniques such as secondary ion mass spectrometry (SIMS) allows analysis of individual spots 30 μ m in diameter or less (Riciputi & Patterson, 1994; Eiler *et al.*, 1997; Vielzeuf *et al.*, 2005a; Page *et al.*, 2010). To test for variations in oxygen isotopic ratios that correlate with changes in compositional zoning patterns in garnet from Passo del Sole, three samples were subjected to SIMS isotopic analysis using the Cameca IMS 1270 ion probe at UCLA.

Selected central sections of garnet from samples PDS03-1, PDS03-2 and AG-4, as located by high-resolution X-ray computed tomography, were carefully trimmed and removed from roughly 100 μ m thick petrographic sections. These individual garnet sections were mounted in clear epoxy, along with geological standard UWG-2 (Valley *et al.*, 1995), and prepared as 2.5 cm round epoxy discs. A separate grain mount containing primary standards AlmCMG, PrpMM, PrpSE, GrsSE and SpeSE (Vielzeuf *et al.*, 2005a,b), prepared using a similar method, was provided by D. Vielzeuf. Care was taken to cluster each crystal or grain to be analysed towards the centre of the block to limit analytical errors due to beam interactions with the edge of the sample holder, as well as systematic geographical errors associated with aiming the beam away from the midpoint of the sample chamber. EPMA mapping and quantitative point analyses on each garnet were used to precisely locate chemical zone boundaries and their distinct chemical compositions (Table 5). Effort was made to colocate microprobe analyses and SIMS point analyses; after analysis, samples were remapped on the microprobe to confirm locations of SIMS analysis pits relative to garnet-zoning patterns. The mounts were polished to provide a flat surface for analysis. Prior to analysis, a thin conductive gold coat was applied. Sputtering employed a spot 30 μ m in diameter, the smallest size compatible with signal requirements.

Analysis of the three Passo del Sole samples took place over the course of two days; primary standards were analysed at the beginning and end of each day to correct analytical errors associated with beam drift. UWG-2, the secondary standard, was analysed after

every four to seven unknowns. Extensive offline corrections are required to counteract the variations in the magnitude of the instrumental mass fractionation (IMF) and matrix effects that result from differences in chemical composition between the unknowns and the standard materials (Eiler *et al.*, 1997; Vielzeuf *et al.*, 2005a). These were performed by calculating matrix coefficients for the IMF associated with each garnet end-member. These coefficients allow the IMF and appropriate correction factor to be calculated for any garnet of intermediate composition. An additional correction was applied to the unknown samples by tracking changes in the measured $\delta^{18}\text{O}$ values for the UWG-2 secondary standard through the course of the day. Replicate analyses of garnet standards indicates precision on the order of $\pm 0.5\text{‰}$ for the garnet analyses reported here.

Oxygen isotopic compositions for garnet from Passo del Sole are presented in Fig. 8. Overall, the magnitude of the isotopic variations from core to rim in these samples is small, and it is difficult to discern distinct patterns in any given sample that are larger in magnitude than the range of possible error in measurement. However, several observations may be made that have implications for the evolution of the fluids seen by each sample during its garnet growth history.

Values of $\delta^{18}\text{O}$ for sample AG-4 (Fig. 8a) are nearly constant from core to rim. Either there was no change in isotopic composition of the fluids accompanying the rapid changes in Ca content that produced the oscillatory zoning patterns, or the length scale of the isotopic oscillations is too small to be effectively isolated and sampled by this technique. Although the larger Ca oscillations in AG-4 are on the order of $50\text{ }\mu\text{m}$ in width, others are $<10\text{ }\mu\text{m}$ wide (Meth & Carlson, 2005). It is certainly possible that the flat $\delta^{18}\text{O}$ profile is the result of averaging zones of heavy and light oxygen that are too fine scaled to measure separately, even using the smallest suitable spot size. Samples PDS03-1 and PDS03-2 – which were collected from the same garnetiferous layer only 5 m apart, but have disparate patterns of compositional zoning (Fig. 5) – show opposite trends in the evolution of their stable isotopes during garnet growth. Values of $\delta^{18}\text{O}$ in PDS03-1 hold

steady at $7\text{--}8\text{‰}$ during the early stages of garnet growth (Fig. 8b: zones 1–3), then jump to nearly $8\text{--}9\text{‰}$ at the position of the outer Mn annulus and abrupt increase in Ca (Fig. 8b: zones 4–5), before finally dropping back to $7.5\text{--}8.5\text{‰}$ in the high-Ca rim (Fig. 8b: zones 6–7). In contrast, the core of sample PDS03-2 has $\delta^{18}\text{O}$ values of $\sim 7\text{‰}$ (Fig. 8c: zone 1) and $\delta^{18}\text{O}$ drops steadily outward: the region of oscillatory Ca has a $\delta^{18}\text{O}$ of $\sim 6.7\text{‰}$ (Fig. 8c: zones 2–4), and $\delta^{18}\text{O}$ in the Ca-poor rim drops to roughly 6‰ (Fig. 8c: zone 5).

These differences between two samples from the same layer cannot be convincingly attributed to variations in fractionation effects between garnet and matrix phases, because the two rocks are lithologically nearly identical. Thus, despite the uncertainties, measured differences in $\delta^{18}\text{O}$ values for these three samples demonstrate that significantly different fluids were present over very short distances during garnet growth. The pronounced differences in fluid composition within the same layer support the hypothesis of punctuated, channelized fluid flow as the likely source of the compositional variation in garnet at Passo del Sole.

Implications for modelling of garnet growth

The foregoing evidence suggests that open-system infiltration of externally derived fluids is responsible for the wide range of compositional variations and modifications that are observed. Before proceeding further, it is important to consider the effects of applying models that assume equilibrium behaviour in a closed system (i.e. THERMOCALC) to rocks that exhibit open-system behaviour for one or more elements. Compositional zoning indicates that rocks near Passo del Sole likely experienced influxes of Ca during garnet growth, as in sample AG-4, or influxes of Ca and Mn during garnet growth, as in sample PDS03-1. The concentric zoning patterns present at Passo del Sole, while providing evidence for fluid-modified compositions, also show that fluids passed through the rock in pulses. After their passage, garnet Ca and Mn compositions returned to values consistent with the closed-

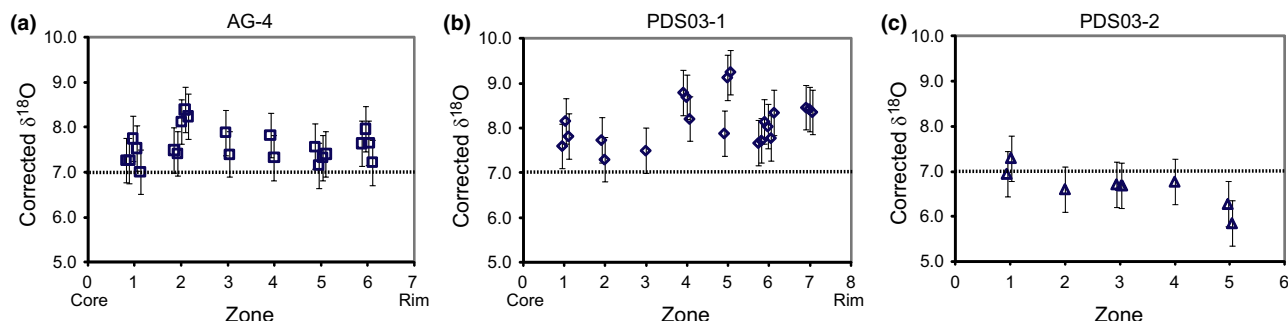


Figure 8. Corrected $\delta^{18}\text{O}$ data for garnet from Passo del Sole. (a) AG-4. (b) PDS03-1. (c) PDS03-2. Zones are specific to each garnet, and are defined in Table 4. Error bars correspond to 0.5‰ reproducibility inherent to technique. See text for discussion.

system regional 'baseline'. Therefore, modification of phase compositions was only a temporary effect produced by the passage of pulses of externally derived fluids, and the effect was isolated to the elements observed to vary sharply in the garnet-zoning patterns; there is little evidence for fluid-assisted modification of other elements used in the MnNCKFMASH thermodynamic model calculations. Attempts to model elements that experienced open-system behaviour as a closed system will undoubtedly produce errors in the equilibrium calculations of phase stability and composition, particularly for crucible phases for these elements. However, externally derived fluids are a common feature in regionally metamorphosed terranes (e.g. Ferry, 1992; Skelton *et al.*, 1995; Ague, 1997); thermodynamic models have long been applied to such systems to investigate their P - T - t evolution. In many cases, fluid-assisted modification of the bulk composition is recorded only by changes in accessory mineral assemblages (e.g. Torres-Ruiz *et al.*, 2003), without obvious breaks in compositional zoning recorded by garnet or other porphyroblast phases. Nevertheless, the open-system character of these rocks may be responsible for some inconsistencies in calculated behaviour described below, such as the failure of all isopleths to intersect precisely at a single point.



Modelling results

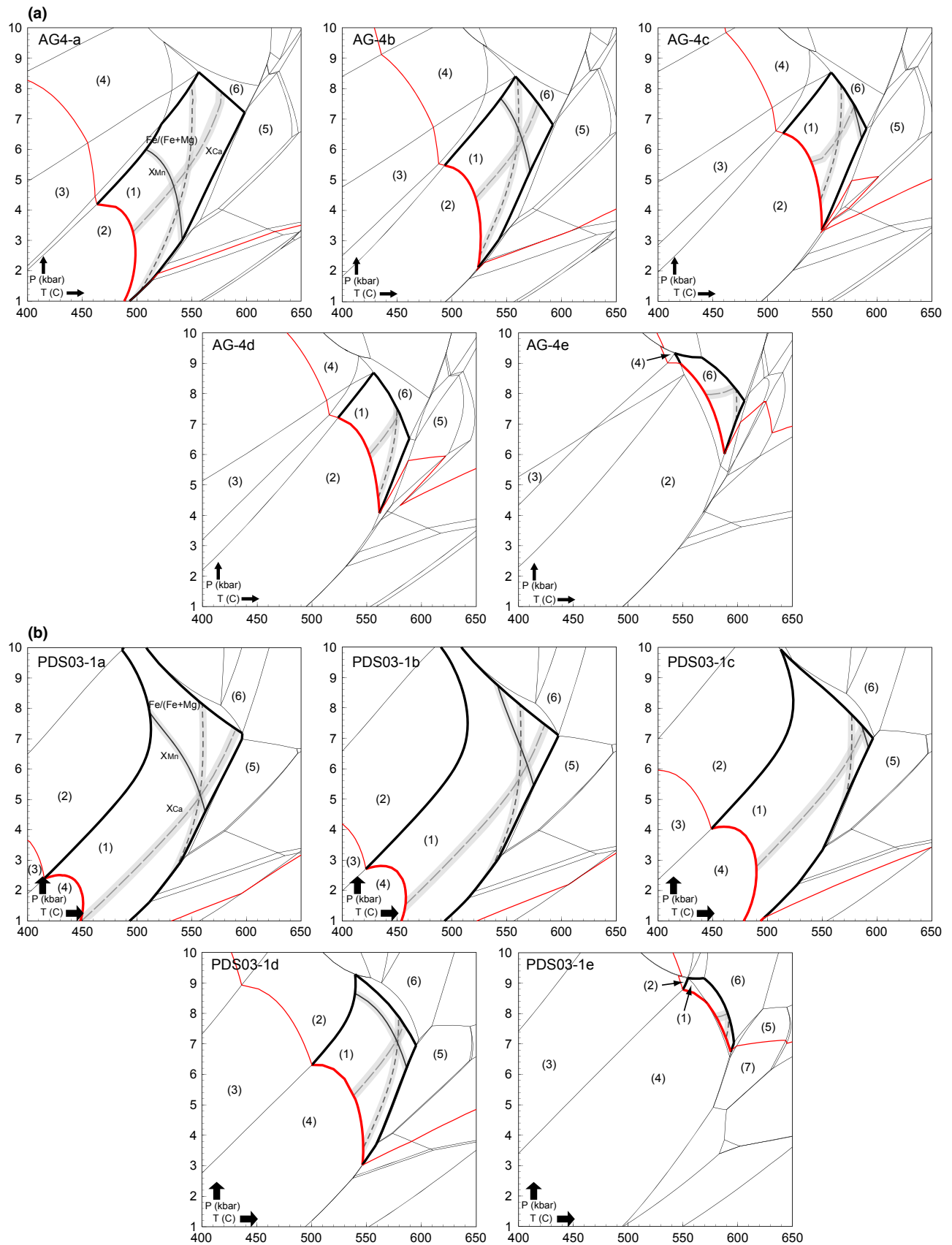
The results of prograde thermal modelling are summarized in Fig. 9a,b, which show the pseudosections produced for AG-4 and PDS03-1 respectively. For both samples, the calculated stable mineral assemblage during prograde growth of garnet is garnet + biotite + chlorite + muscovite + plagioclase + quartz + H_2O . Except for trace amounts ($\leq 1\%$) of staurolite and kyanite in Sample AG-4, the calculated assemblage matches observation well. The evolution of P - T conditions during garnet growth, based on the intersections of $Fe/(Fe + Mg)$, X_{Ca} , X_{Mn} garnet isopleths in successive pseudosections, shows that temperature increased continuously throughout the entire garnet growth history. Although the positions of the X_{Ca} and X_{Mn} garnet isopleths may be adversely affected to some degree by transient open-system behaviour during some stages of garnet

growth, as noted above, the temperature values are tightly constrained by the $Fe/(Fe + Mg)$ isopleth which, in the pressure ranges previously measured for this region of the Alps, changes little as a function of pressure, and behaves essentially as a geothermometer. Temperatures recorded for each garnet growth stage were determined by the intersection point of the X_{Ca} and/or X_{Mn} garnet isopleths with the $Fe/(Fe + Mg)$ isopleth. Setting aside the uncertainties associated with the *absolute* temperatures of equilibration calculated by the model, two observations indicate that the *relative* temperature changes modelled for each sample are accurate: (i) each stage of garnet growth in each sample is associated with an increase in calculated temperature, regardless of open-system behaviour in Ca or Mn; and (ii) although the original bulk compositions for each sample are somewhat different, and garnet growth begins quite plausibly at different temperatures in each sample, the last stages of garnet growth in each sample are calculated at 600 °C by the model (Fig. 10). This implies that despite differences in bulk composition, timing of initiation of garnet growth, and likely differences in open-system fluid chemistries, the model was able to correlate the thermal conditions present during the last stages of garnet growth in each sample. It may be safely concluded that any systematic errors in calculated temperatures are consistent throughout the pseudosections, so that relative changes in temperature between intervals of garnet growth, which are the important values to consider for calculations of garnet growth rate and strain rate, are likely to be accurate.

Measurements of inclusion-trail curvature

The amount of deflection of inclusion trails was measured for three centrally sectioned porphyroblasts in each of samples AG-4 and PDS03-1. For sample PDS03-1, apparent garnet rotations for successive stages of garnet growth were determined from photomicrographs overlain by compositional X-ray maps, due to the fine-grained nature of the inclusions. For sample AG-4, apparent garnet rotations were measured from Ca X-ray maps of centrally sectioned porphyroblasts prepared for previous study (Meth & Carlson, 2005); most garnet crystals that had been

Figure 9. (a) MnNCKFMASH pseudosections calculated for sample AG-4. Heavy lines outline stability field of observed peak assemblage during garnet growth. Medium-weight  lines show position of garnet-in reaction curves. Equilibrium temperatures for each stage of garnet growth are calculated from the intersection of garnet isopleths: X_{Ca} (long-dashed line), X_{Mn} (solid line) and $Fe/(Fe + Mg)$ (short-dashed line); shaded regions represent ± 0.01 error envelope for calculated isopleth values. Quartz + H_2O are present in excess. Numbered fields in pseudosections refer to mineral assemblages: (1) Grt + Bt + Chl + Pl + Ms; (2) Bt + Chl + Pl + Ms; (3) Zo + Chl + Pl + Ms; (4) Grt + Zo + Chl + Pl + Ms; (5) Stt + Grt + Bt + Pl + Ms; (6) Grt + Bt + Chl + Par + Pl + Ms. (Key to abbreviations: Grt, garnet; Stt, staurolite; Bt, biotite; Chl, chlorite; Ms, muscovite; Pl, plagioclase; Zo, zoisite; Par, paragonite; Qtz, quartz). (b) MnNCKFMASH pseudosections calculated for sample PDS03-1. Heavy lines outline stability field of observed peak assemblage during garnet growth. Medium-weight  lines show position of garnet-in reaction curves. Equilibrium temperatures for each stage of garnet growth (a–e) are calculated from the intersection of garnet isopleths: X_{Ca} (light-grey dashed line), X_{Mn} (solid line) and $Fe/(Fe + Mg)$ (medium-grey short-dashed line). Quartz + H_2O are present in excess. Numbered fields in pseudosections refer to mineral assemblages: (1) Grt + Bt + Chl + Pl + Ms; (2) Grt + Zo + Bt + Chl + Pl + Ms; (3) Zo + Bt + Chl + Pl + Ms; (4) Bt + Chl + Pl + Ms; (5) Stt + Grt + Bt + Pl + Ms; (6) Grt + Bt + Par + Pl + Ms; (7) Stt + Bt + Pl + Ms. Mineral abbreviations as in (a).



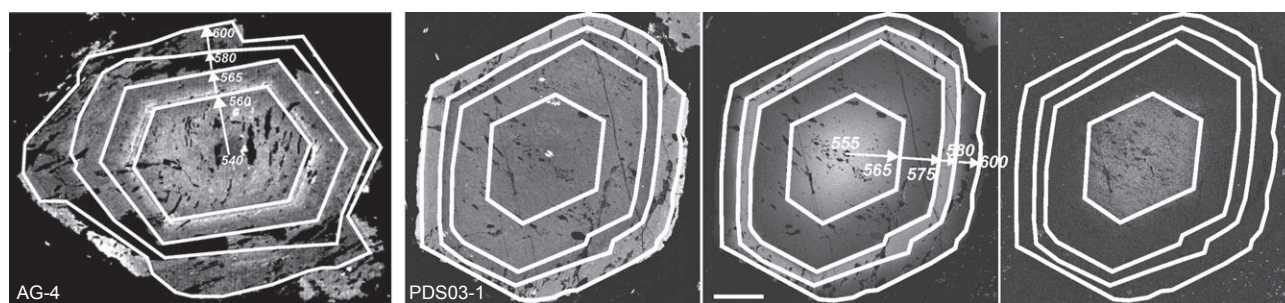


Figure 10. Summary of thermal models for the prograde growth of garnet at Passo del Sole overlain on the garnet growth zones described in the text.

previously analysed had been destroyed by progressive grinding through the sample. The results of measurements of inclusion-trail curvature are included in Table 6.

STRAIN-RATE CALCULATIONS

Rotational case

The estimation of heating rates, a key component of this method of strain-rate calculation, is commonly problematic; rarely is the prograde segment of the T - t path

Combining the three parameters listed above, the strain rate during the growth of garnet porphyroblasts can be calculated from the relationship

$$\dot{\gamma} = (h/\Delta T) * 2\omega$$

in which $\dot{\gamma}$ is the strain rate, h is the heating rate, ΔT is the change in temperature during an interval of garnet growth and ω is the magnitude of apparent rotation during that interval. Strain rates calculated for the entire crystallization interval, and for individual stages of garnet growth, are shown in Table 7.

At Passo del Sole, the strain rate averaged over the entire prograde garnet growth interval is between 1.9×10^{-14} and $4.8 \times 10^{-14} \text{ s}^{-1}$, depending on the value chosen for the heating rate. Comparison with previous strain-rate calculations shows that the values obtained in this study are in general agreement with the range of values that have been reported in the literature, and confirms the effectiveness of the Biermeier & Stüwe (2003) approach.

In this study, however, it also proved possible to obtain individual strain rates for multiple short intervals of garnet growth, a level of time-resolved detail not achieved in previous studies. This high temporal resolution, which is of course a measure of relative time – not absolute time – was attainable because of the precise characterization of garnet nucleation and growth mechanisms and the presence of compositional variations acting as time markers during garnet growth. Analyses of inclusion-trail deflection for multiple garnet crystals from AG-4 and PDS03-1 reveal systematic variations in the strain rates during garnet growth (Fig. 11, Table 7) that correlate directly with zones of unusual garnet composition. Within each zone, excellent agreement is seen for each of the three crystals analysed; these internal variations give an idea of the level of precision to be expected from this approach. Importantly, in each sample, all three crystals record substantial increases in strain rate during those portions of the garnet growth history that produced marked excursions in garnet chemistry, followed by an abrupt return to prior rates. In sample AG-4, there is a twofold increase in the measured strain rate at the zone corresponding to the high-Ca spike (growth interval

Table 6. Inclusion deflection measurements, in degrees.

Sample	AG-4			PDS03-1		
	g4	g19	g23	g64	g60-1	g41
Growth interval A ^a	47	15	88	17	9	22
Growth interval B	29	14	23	15	24	38
Growth interval C	43	12	10	32	61	35
Growth interval D	19	45	44	30	44	61
Growth interval E	– ^b	–	–	5	19	–

^aRefer to text for growth interval definitions.

^bDeflection not measured in some garnet crystals due to discontinuous nature of Growth Interval E in most crystals.

preserved. One approximation that has been used is to assume that heating rates during regional metamorphism are equivalent to cooling rates (e.g. England & Thompson, 1984); this approximation was used by Biermeier & Stüwe (2003) in their calculations. However, in this instance, direct determinations of the regional prograde heating rate have been made. Vance & O'Nions (1992) report heating rates of 12 °C Ma^{-1} in the western Lepontine Alps, based on U–Pb, Sm–Nd and Rb–Sr garnet geochronology. For the northern Lepontine Dome, Janots *et al.* (2009) determined heating rates based on accessory phase stability and geochronology that fall in the range 8 – 15 °C Ma^{-1} . In the analysis that follows, strain rates are calculated on the basis of a heating rate of $11.5 \pm 3.5 \text{ °C Ma}^{-1}$, a value in the centre of the range given by Janots *et al.* (2009) with a corresponding uncertainty; this value is also consistent with the estimate of Vance & O'Nions (1992).

Table 7. Strain-rate calculations for garnet growth at Passo del Sole.

Sample		AG-4								
Crystal		g4			g19			g23		
Growth interval	ΔT ($^{\circ}\text{C}$)	$\Delta\theta$ ($^{\circ}$)	Strain rate (10^{-14} s^{-1})	Uncertainty (10^{-14} s^{-1})	$\Delta\theta$ ($^{\circ}$)	Strain rate (10^{-14} s^{-1})	Uncertainty (10^{-14} s^{-1})	$\Delta\theta$ ($^{\circ}$)	Strain rate (10^{-14} s^{-1})	Uncertainty (10^{-14} s^{-1})
A–B	20	47	3.0	0.9	15	1.0	0.3	88	5.6	1.7
B–C	5	29	7.4	2.2	14	3.6	1.1	23	5.9	1.7
C–D	15	43	3.6	1.1	12	1.0	0.3	10	0.9	0.3
D–E	20	19	1.2	0.4	45	2.9	0.9	44	2.8	0.9

Sample		PDS03-1								
Crystal		g41			g60-1			g64		
Growth interval	ΔT ($^{\circ}\text{C}$)	$\Delta\theta$ ($^{\circ}$)	Strain rate (10^{-14} s^{-1})	Uncertainty (10^{-14} s^{-1})	$\Delta\theta$ ($^{\circ}$)	Strain rate (10^{-14} s^{-1})	Uncertainty (10^{-14} s^{-1})	$\Delta\theta$ ($^{\circ}$)	Strain rate (10^{-14} s^{-1})	Uncertainty (10^{-14} s^{-1})
A–B	10	22	2.8	0.9	9	1.1	0.3	17	2.2	0.6
B–C	10	38	4.8	1.4	24	3.1	1.0	15	1.9	0.6
C–D	5	35	8.9	2.7	61	16.0	4.5	32	8.1	2.4
D–E	20	61	3.9	1.2	44	2.8	0.9	30	1.9	0.6

Strain rates and their uncertainties are based on heating rate $h = 11.5 \pm 3.5 \text{ }^{\circ}\text{C Ma}^{-1}$ (Janots *et al.*, 2009).

B–C). Likewise, in sample PDS03-1, there is a threefold to fivefold increase in the measured strain rate (up to $16 \times 10^{-14} \text{ s}^{-1}$) at the zone corresponding to the high-Mn annulus (growth interval C–D). These samples were obtained in close proximity ($\sim 35 \text{ m}$ apart) and must share the same thermal and tectonic history, yet the high strain-rate zones grew at different temperatures and thus different times.

It is conceivable, of course, that the anomalies we regard as variations in strain rate at near-constant heating rate might instead reflect variations in heating rate at near-constant strain rate; this mechanism could produce patterns of garnet growth similar to those observed in these samples (cf. Pollington & Baxter, 2010). We consider that alternative as implausible for three reasons. First, the magnitude of the required changes in heating rate is quite large: the heating rate at constant strain rate needed to explain the anomalies ranges up to $60 \text{ }^{\circ}\text{C Ma}^{-1}$, rising from and returning to a background of $11.5 \text{ }^{\circ}\text{C Ma}^{-1}$ across very short intervals of growth. It is difficult to envisage a mechanism that could effect such large, rapid, short-lived changes in heating rate for rocks deeply buried in the crust. Second, the required abrupt changes in heating rates would have to have occurred at different temperatures and thus at different times in rocks only metres apart. Again, no credible mechanism to achieve such spatial variations presents itself for rocks in the deep crust. Third, and perhaps most persuasively, we can conceive of no tenable means by which large, transient chemical changes of two different types (Ca v. Mn influx) can be induced simply by increasing then decreasing the heating rate; these chemical variations that correlate directly with increases in apparent rate of garnet rotation are far more easily explained by episodic introduction of reactive fluids.

We therefore interpret the correlation between increases in strain rate and zones of unusual chemical

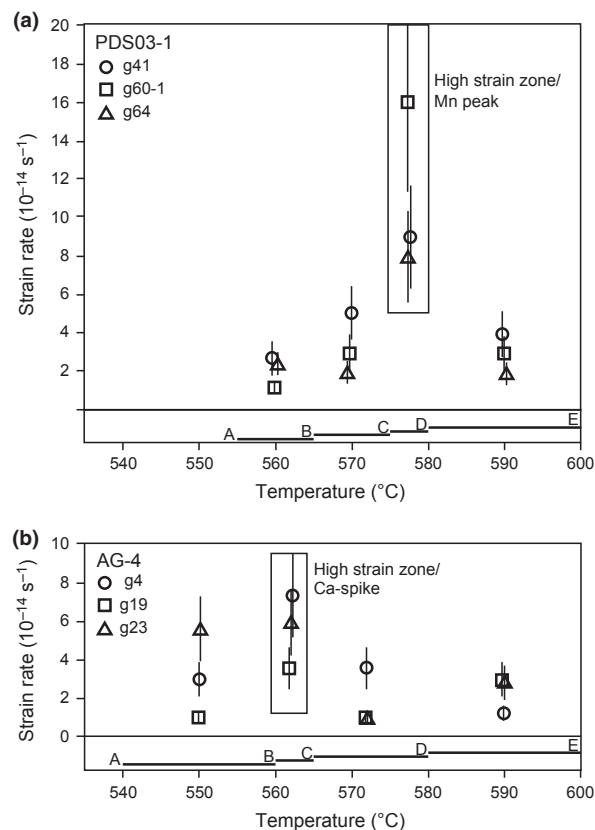


Figure 11. Changes in strain rate during prograde garnet growth (assumed heating rate of $11.5 \text{ }^{\circ}\text{C Ma}^{-1}$) for selected garnet from samples (a) PDS03-1 and (b) AG-4. A–B, B–C, C–D, D–E bars refer to the garnet growth zones defined in the text. Error bars correspond to the uncertainties in heating rates ($\pm 3.5 \text{ }^{\circ}\text{C Ma}^{-1}$) for the northern Lepontine Dome as estimated by Janots *et al.* (2009). Apparent peaks in strain rate can be correlated to garnet growth zones associated with the unusual garnet-zoning patterns in each sample. Outside anomalous zones, strain-rate values for both samples are very similar. See text for further discussion.

composition in garnet to be the result of infiltration of metamorphic fluids along the shear-zone boundary that modified the system's bulk chemistry while inducing strain softening that accelerated strain. Fluids are known to affect rock rheology and to enhance strain rates in a variety of metamorphic settings (e.g. Williams, 1994; Zulauf & Helfferich, 1997). The passage of fluids, and resultant strain softening and rheological weakening, is commonly observed along shear-zone boundaries (e.g. McCaig, 1984; Selverstone *et al.*, 1991; Fletcher, 1998; Yonkee *et al.*, 2003). Rocks in shear zones do not behave uniformly during deformation; they are subjected to regimes of alternating strengthening and weakening during metamorphism (Steffen *et al.*, 2000). Selverstone *et al.* (1991) observed evidence for the channelization of fluids during ductile shearing in the Eastern Alps.

At Passo del Sole, we document wide variations in garnet zoning and strain rate, not only from one lithological layer to another, but also between samples within the same layer separated by only a few metres along strike. These features appear at different times during the garnet growth history in neighbouring samples, so the inference that they are fluid induced requires fluid flow that was episodic in nature and channelized, not necessarily only within individual layers but likely across layers as well.

As this study was being prepared for final publication, additional work done by Stacy (2012) on samples from the same locality – using nearly identical techniques – provided additional confirmation of this hypothesis. First, one sample that showed no evidence of fluid infiltration during garnet growth (no anomalous cation zoning) exhibited no elevation of strain rates; instead, strain rates throughout garnet growth remained at the same low levels observed in this study for regions outside compositional anomalies. This provides an important 'control' sample, confirming that elevated strain rates occur only when compositional anomalies are introduced. Second, strain-rate analysis of sample PDS03-2 of this study, which was collected from the same garnetiferous layer as PDS03-1 but 5 m distant along strike, and which exhibits distinctly different chemical-zoning patterns in garnet (i.e. high-Ca zones rather than high-Mn zones), showed that both sets of compositional anomalies are associated with elevated strain rates.

The non-rotational case

An alternative hypothesis for the formation of curved inclusion trails in garnet is that they are produced by progressive growth of garnet over successive orthogonal matrix foliations. According to this interpretation, the garnet remains stationary as the matrix deforms around it, and stages of porphyroblast growth are restricted to regimes in which deformation is not active (Bell, 1985; Bell *et al.*, 1992a,b; Hayward, 1992). Spiral inclusion textures are thus envisioned to form by gar-

net overgrowing multiple matrix foliations, with growth hiatuses during episodes of deformation and foliation development. These interruptions in garnet growth may not be recorded by obvious breaks in the compositional zoning patterns of the porphyroblast (Stallard & Hickey, 2002). Obviously, for rocks to which this non-rotational model applies, the interaction between a porphyroblast and the deforming matrix cannot be described by the foregoing relationship between rotation rate and strain rate. Although this interpretation may be falling into disfavour (cf. Johnson, 2009), we also estimated strain rates assuming non-rotation of porphyroblasts during growth were also performed, to provide an informative comparison.

Johnson & Williams (1998) estimated the amount of strain required to produce new metamorphic fabrics, such as those that can be observed in the interiors of garnet porphyroblasts, by comparing the spacing between foliation surfaces in garnet interiors with the spacing between the same surfaces in the surrounding matrix. The study examined the strain associated with the X, Y and Z directions of the finite-strain ellipsoid to determine the amount of shortening required to produce the observed textures. For the end-member case of a plane-strain shearing environment in which all deformation is along one directional axis – comparable to the likely deformational environment active at Passo del Sole during garnet growth – the total maximum strain associated with the development of a new metamorphic foliation is 0.63 (Johnson & Williams, 1998).

An obstacle to applying this method to the garnet crystals examined in this study is that Passo del Sole garnet lacks the oppositely concave microfolds preserved as inclusions that were utilized by Johnson & Williams (1998). Garnet crystals in this study exhibit evidence for more than one episode of new foliation development during growth of the porphyroblast: measured changes in inclusion-trail orientation approach 180° in sample AG-4. It is difficult to track foliation surfaces between cores of garnet porphyroblasts and the external fabrics. However, there are alternative means of estimating the amount of strain during metamorphism. Examination of plagioclase feldspar crystals in the matrix of sample PDS03-1 shows that these crystals have developed compositional zoning (Fig. 12). Internal zoning patterns are circular in cross-section, whereas the crystal morphology, which has been affected by dynamic recrystallization processes in the deforming matrix, is strongly elliptical and elongated. Comparison of the aspect ratios of feldspar cores, as determined by the observed compositional zoning patterns, with the current grain shape reveals that plagioclase aspect ratios have changed by 64%. Although garnet crystals from the samples included in this study lack definitive millipede structures or other internal features that demonstrate the amount of strain during metamorphism (e.g. Johnson, 1999), the directional-strain model may be used as a benchmark.

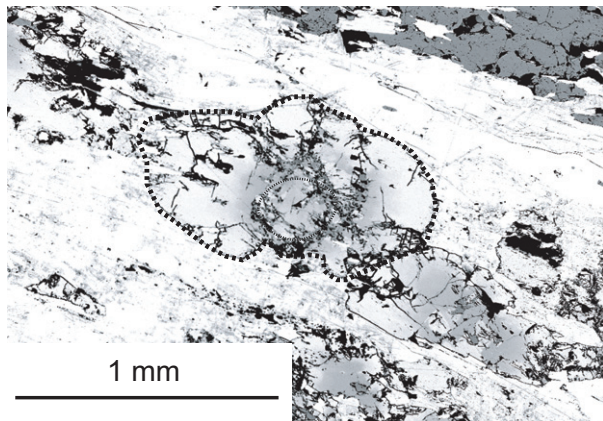


Figure 12. BSE image of plagioclase crystal in sample PDS03-1. The long axis of the plagioclase crystal is parallel to the dominant matrix foliation; elongate crystal shapes with circular compositional zoning preserved in feldspar interiors allow independent estimation of strain associated with shearing during metamorphism at Passo del Sole.

Strain-rate estimates for development of orthogonal foliations associated with 60% shortening and heating rates in the range $8\text{--}15\text{ }^{\circ}\text{C Ma}^{-1}$ are listed in Table 8. These values are smaller by a factor of three than those produced using the Biermeier & Stüwe (2003) approach, but values approaching $1 \times 10^{-14}\text{ s}^{-1}$ during garnet growth for samples AG-4 and PDS03-1 are quite close to the average strain-rate values measured for the intervals of garnet growth that are not associated with the unusual garnet-zoning patterns (strain softening). If the non-rotational model proposed by Bell *et al.* (1992b) holds, then the rheological relationships used to describe the rotation of the growing garnet within the deforming matrix, which form the basis for rotational strain-rate calculations, cannot be correct. The near-agreement between strain rates measured by rotational and non-rotational techniques may then be merely coincidental. It is also possible, however, that the near agreement indicates that both postulated processes are governed fundamentally by the same underlying physical phenomena (the matrix rheology), so that both approaches tend to converge to a similar result.

SUMMARY AND CONCLUSIONS

The strain-rate calculation method developed by Biermeier & Stüwe (2003) has been shown to be a highly effective means of estimating prograde strain rates at the hand-sample scale and has the potential to become a powerful tool for quantifying rheological evolution during metamorphism, particularly if one is able to sufficiently characterize the conditions and processes that control garnet growth. Garnetiferous samples from Passo del Sole have proven to be especially well suited to strain-rate calculations due to their chemical-zoning patterns, including high-Ca oscillations and

Table 8. Strain-rate calculations for the non-rotational case.

Sample	AG-4		PDS03-1
	1st foliation ^a	2nd foliation ^b	New foliation ^c
T range ^d	540–565	565–600	555–580
ΔT ($^{\circ}\text{C}$)	25	35	25
Strain rate ^e	$8.7 \pm 2.6 \times 10^{-15}$	$6.2 \pm 1.9 \times 10^{-15}$	$8.7 \pm 2.6 \times 10^{-15}$

^aFormation of first orthogonal fabric after 90° of inclusion trail curvature.

^bFormation of second orthogonal fabric after 180° of inclusion trail curvature.

^cFormation of new orthogonal fabric after 90° of inclusion trail curvature.

^dAs determined by pseudosection thermometry.

^eBased on heating rates of $11.5 \pm 3.5\text{ }^{\circ}\text{C Ma}^{-1}$ (Janots *et al.*, 2009).

high-Mn annuli, which allow compositional and textural correlation among porphyroblasts throughout the hand specimen. These correlations allow each zone to serve as a time marker during garnet growth, and along with identification of the specific mechanism controlling crystal growth, they greatly reduce the uncertainties associated with the various assumptions required by the method, while eliminating some entirely. This markedly increases the accuracy of the garnet growth models, reduces the error on strain-rate estimates derived from them and allows higher resolution analysis of strain rates during garnet growth than has been possible previously. At Passo del Sole, twofold to fivefold variations in strain rate are correlated with the unusual compositional zoning in garnet, pointing towards fluid-assisted strain softening as the likely cause for elevated strain rates. Garnet crystals at this locality therefore preserve quantifiable, time-resolved evidence for short-term, localized variations in rheology during deformation and metamorphism.

ACKNOWLEDGEMENTS

We thank M. Grove and A. Schmidt for guiding the SIMS analyses at UCLA, L. Baumgartner for pointing out the potential for pre-Alpine crystallization, and S. Johnson for his advice on carrying out the non-rotational strain-rate calculations. D. Vielzeuf very kindly loaned his set of garnet oxygen-isotope standards for our use during the SIMS analyses. E. Baxter and an anonymous reviewer provided advice that greatly improved the manuscript. We also thank the Museo Cantonale di Storia Naturale, Lugano, Switzerland, for granting permission to collect specimens from the natural preserve in which Passo del Sole is located.

REFERENCES

- Ague, J.J., 1997. Crustal mass transfer and index mineral growth in Barrow's garnet zone, Northeast Scotland. *Geology*, **25**, 73–76.
- Barker, A.J., 1994. Interpretation of porphyroblast inclusion trails: limitations imposed by growth kinetics and strain rates. *Journal of Metamorphic Geology*, **12**, 681–694.
- Baxter, E.F. & DePaolo, D.J., 2004. Can metamorphic reactions proceed faster than bulk strain? *Contributions to Mineralogy and Petrology*, **146**, 657–670.

- Bell, T.H., 1985. Deformation partitioning and porphyroblast rotation in metamorphic rocks: a radical reinterpretation. *Journal of Metamorphic Geology*, **3**, 109–118.
- Bell, T.H., Forde, A. & Hayward, N., 1992a. Do smoothly curved, spiral-shaped inclusion trails signify porphyroblast rotation? *Geology*, **20**, 59–62.
- Bell, T.H., Johnson, S.E., Davis, B. *et al.*, 1992b. Porphyroblast inclusion-trail orientation data: eppure non son girate! *Journal of Metamorphic Geology*, **10**, 295–307.
- Berg, C.A., 2007. Strain Rates and Constraints on Chemical Homogeneity and Length Scales of Equilibration During Alpine Metamorphism at Passo del Sole, Central Swiss Alps. Ph.D Dissertation, The University of Texas at Austin, Austin, TX, 357 pp.
- Biermeier, C. & Stüwe, K., 2003. Strain rates from snowball garnet. *Journal of Metamorphic Geology*, **21**, 253–268.
- Biermeier, C., Stüwe, K. & Barr, T.D., 2001. The rotation rate of cylindrical objects during simple shear. *Journal of Structural Geology*, **23**, 765–776.
- Busa, M.D. & Gray, N.H., 2005. Fan-shaped staurolite in the Bolton syncline, eastern Connecticut: evidence for porphyroblast rotation during growth. *Journal of Metamorphic Geology*, **23**, 881–895.
- Carlson, W.D. & Denison, C., 1992. Mechanisms of porphyroblast crystallization: results from high-resolution computed X-ray tomography. *Science*, **257**, 1236–1239.
- Chadwick, B., 1968. Deformation and metamorphism in the Lukmanier region, central Switzerland. *Geological Society of America Bulletin*, **79**, 1123–1150.
- Chamberlain, C.P. & Conrad, M.E., 1991. Oxygen isotope zoning in garnet. *Science*, **254**, 403–406.
- Christensen, J.N., Rosenfeld, J.L. & DePaolo, D.J., 1989. Rates of tectonometamorphic processes from rubidium and strontium isotopes in garnet. *Science*, **244**, 1465–1469.
- Christensen, J.N., Selverstone, J., Rosenfeld, J.L. & DePaolo, D.J., 1994. Correlation by Rb–Sr geochronology of garnet growth histories from different structural levels within the Tauern Window, Eastern Alps. *Contributions to Mineralogy and Petrology*, **118**, 1–12.
- Connelly, J.N., 2006. Improved dissolution and chemical separation methods for Lu–Hf garnet chronometry. *Geochemistry Geophysics Geosystems*, **7**, 1–9.
- Denison, C. & Carlson, W.D., 1997. Three-dimensional quantitative textural analysis of metamorphic rocks using high-resolution computed X-ray tomography: Part II. Application to natural samples. *Journal of Metamorphic Geology*, **15**, 45–57.
- Eiler, J.M., Graham, C. & Valley, J.W., 1997. SIMS analysis of oxygen isotopes: matrix effects in complex minerals and glasses. *Chemical Geology*, **138**, 221–244.
- England, P.C. & Thompson, A.B., 1984. Pressure-temperature-time paths of regional metamorphism: I. Heat transfer during the evolution of regions of thickened continental crust. *Journal of Petrology*, **25**, 894–928.
- Evans, T.P., 2004. A method for calculating effective bulk composition modification due to crystal fractionation in garnet-bearing schist: implications for isopleth thermobarometry. *Journal of Metamorphic Geology*, **22**, 547–557.
- Ferry, J.M., 1992. Regional metamorphism of the Waits River Formation, eastern Vermont: delineation of a new type of giant metamorphic hydrothermal system. *Journal of Petrology*, **33**, 45–94.
- Fletcher, R.C., 1998. Effects of pressure solution and fluid migration on initiation of shear zones and faults. *Tectonophysics*, **295**, 139–165.
- Frey, M. & Mählmann, R.F., 1999. Alpine metamorphism of the Central Alps. *Schweizerische Mineralogische und Petrographische Mitteilungen*, **79**, 135–154.
- Frey, M., Trommsdorff, V. & Wenk, E., 1980. Alpine metamorphism of the Central Alps. In: *Geology of Switzerland, Part B: Geological Excursions* (ed. Trump, R.), pp. 295–316. Wepf & Company, New York.
- Hayward, N., 1992. Microstructural analysis of the classic snowball garnets of southeast Vermont: evidence for non-rotation. *Journal of Metamorphic Geology*, **10**, 567–587.
- Holland, T.J.B. & Powell, R., 1990. An enlarged and updated internally consistent thermodynamic dataset with uncertainties and correlations: the system K_2O – Na_2O – CaO – MgO – MnO – FeO – Fe_2O_3 – Al_2O_3 – TiO_2 – SiO_2 – C – H_2 – O_2 . *Journal of Metamorphic Geology*, **8**, 89–124.
- Holm, D.K. & Selverstone, J., 1990. Rapid growth and strain rates inferred from synkinematic garnets, Penokean orogeny, Minnesota. *Geology*, **18**, 166–169.
- Janots, E., Engi, M., Rubatto, D., Berger, A., Gregory, C. & Rahn, M., 2009. Metamorphic rates in collisional orogeny from *in situ* allanite and monazite dating. *Geology*, **37**, 11–14.
- Johnson, S.E., 1999. Porphyroblast microstructures: a review of current and future trends. *American Mineralogist*, **84**, 1711–1726.
- Johnson, S.E., 2009. Porphyroblast rotation and strain localization: debate settled! *Geology*, **37**, 663–666.
- Johnson, S.E. & Williams, M.L., 1998. Determining finite longitudinal strains from oppositely-concave microfolds in and around porphyroblasts: a new quantitative method. *Journal of Structural Geology*, **20**, 1521–1530.
- Johnson, C.M., Shirey, S.B. & Barovich, K.M., 1996. New approaches to crustal evolution studies and the origin of granitic rocks: what can the Lu–Hf and Re–Os isotopic systems tell us? *Geological Society of America Special Paper*, **315**, 339–352.
- Johnson, S.E., Dupee, M.E. & Guidotti, C.V., 2006. Porphyroblast rotation during crenulation cleavage development: an example from the aureole of the Mooselookmeguntic pluton, Maine, USA. *Journal of Metamorphic Geology*, **24**, 55–73.
- Kohn, M.J., Valley, J.W., Elsenheimer, D. & Spicuzza, M.J., 1993. O isotope zoning in garnet and staurolite: evidence for closed-system mineral growth during regional metamorphism. *American Mineralogist*, **78**, 988–1001.
- Lanzirotti, A., 1995. Yttrium zoning in metamorphic garnets. *Geochimica et Cosmochimica Acta*, **59**, 4105–4110.
- Lapen, T.J., Johnson, C.M., Baumgartner, L.P., Mahlen, N.J., Beard, B.L. & Amato, J.M., 2003. Burial rates during prograde metamorphism of an ultra-high-pressure terrane: an example from Lago di Cignana, Western Alps, Italy. *Earth and Planetary Science Letters*, **215**, 57–72.
- Lapen, T.J., Johnson, C.M., Baumgartner, L.P. *et al.*, 2007. Coupling of oceanic and continental crust during Eocene eclogite-facies metamorphism: evidence from the Monte Rosa nappe, Western Alps. *Contributions to Mineralogy and Petrology*, **153**, 139–157.
- Masuda, T. & Mochizuki, S., 1989. Development of snowball structure: numerical simulation of inclusion trails during synkinematic porphyroblast growth in metamorphic rocks. *Tectonophysics*, **170**, 141–150.
- McCaffrey, R., 1996. Estimates of modern arc-parallel strain rates in fore arcs. *Geology*, **24**, 27–30.
- McCaig, A.M., 1984. Fluid-rock interaction in some shear zones from the Pyrenees. *Journal of Metamorphic Geology*, **2**, 129–141.
- Meth, C.E. & Carlson, W.D., 2005. Diffusion-controlled synkinematic growth of garnet from a heterogeneous precursor at Passo del Sole, Switzerland. *The Canadian Mineralogist*, **43**, 157–182.
- Müller, W., Aerden, D. & Halliday, A.N., 2000. Isotopic dating of strain fringe increments: duration and rates of deformation in shear zones. *Science*, **288**, 2195–2198.
- Page, F.Z., Kita, N.T. & Valley, J.W., 2010. Ion microprobe analysis of oxygen isotopes in garnets of complex chemistry. *Chemical Geology*, **270**, 9–19.
- Passchier, C.W., Trouw, R.A.J., Zwart, H.J. & Vissers, R.L.M., 1992. Porphyroblast rotation: eppur si muove? *Journal of Metamorphic Geology*, **10**, 283–294.

- Paterson, S.R. & Tobisch, O.T., 1992. Rates of processes in magmatic arcs: implications for the timing and nature of pluton emplacement and wall rock deformation. *Journal of Structural Geology*, **14**, 291–300.
- Pfiffner, O.A. & Ramsay, J.G., 1982. Constraints on geological strain rates: arguments from finite strain states of naturally deformed rocks. *Journal of Geophysical Research B*, **87**, 311–321.
- Pollington, A.D. & Baxter, E.F., 2010. High resolution Sm-Nd garnet geochronology reveals the uneven pace of tectono-metamorphic processes. *Earth and Planetary Science Letters*, **293**, 63–71.
- Powell, R. & Holland, T.J.B., 1988. An internally consistent dataset with uncertainties and correlations: 3. Applications to geobarometry, worked examples and a computer program. *Journal of Metamorphic Geology*, **6**, 173–204.
- Powell, R., Holland, T.J.B. & Worley, B., 1998. Calculating phase diagrams involving solid solutions via non-linear equations, with examples using THERMOCALC. *Journal of Metamorphic Geology*, **16**, 577–588.
- Riciputi, L.R. & Paterson, B.A., 1994. High spatial resolution measurement of O isotope ratios in silicates and carbonates by ion microprobe. *American Mineralogist*, **79**, 1227–1230.
- Rosenfeld, J.L., 1970. Rotated garnets in metamorphic rocks. *Geological Society of America Special Paper*, **129**, 105 pp.
- Rosenfeld, J.L., 1987. Rotating garnets. In: *Encyclopedia of Structural Geology*, Vol. X (ed. Seyfert, C.K.), pp. 702–709. Van Nostrand Reinhold Company, New York.
- Scherer, E.E., Cameron, K.L. & Blichert-Toft, J., 2000. Lu-Hf garnet geochronology: closure temperature relative to the Sm-Nd system and the effects of trace mineral inclusions. *Geochimica et Cosmochimica Acta*, **64**, 3413–3432.
- Schoeneveld, C., 1977. A study of typical inclusion patterns in strongly paracrystalline-rotated garnets. *Tectonophysics*, **39**, 453–471.
- Selverstone, J., Morteau, G. & Staude, J.M., 1991. Fluid channeling during ductile shearing: transformation of granulite into aluminous schist in the Tauern Window, Eastern Alps. *Journal of Metamorphic Geology*, **9**, 419–431.
- Skelton, A.D.L., Graham, C.M. & Bickle, M.L., 1995. Lithological and structural controls on regional 3-D fluid flow patterns during greenschist facies metamorphism of the Dalradian of the SW Scottish Highlands. *Journal of Petrology*, **36**, 563–586.
- Skelton, A., Annersten, H. & Valley, J., 2002. $\delta^{18}\text{O}$ and yttrium zoning in garnet: time markers for fluid flow? *Journal of Metamorphic Geology*, **20**, 457–466.
- Stacy, S., 2012. Evidence from high-temporal-resolution strain rates for strain softening due to episodic fluid influx at Passo del Sole, Central Swiss Alps. M.S. Thesis, The University of Texas at Austin, Austin, TX, 163 pp.
- Stallard, A. & Hickey, K., 2002. A comparison of microstructural and chemical patterns in garnet from the Fleur de Lys Supergroup, Newfoundland. *Journal of Structural Geology*, **24**, 1109–1123.
- Steffen, K.J., Selverstone, J. & Brearley, A., 2000. Evidence of progressive weakening and strengthening due to the interaction of metamorphic and deformational processes in a lower crustal shear zone in the Alps. *Geological Society of America Abstracts with Programs*, **32**, 98.
- Stowell, H.H., Tinkham, D.K. & Zuluaga, C.A., 2005. Quantitative P-T-t paths from integrated thermodynamic modeling and metamorphic textures: a short course manual. *Cordilleran Section of the Geological Society of America*, 87.
- Stüwe, K., 1997. Effective bulk composition changes due to cooling: a model predicting complexities in retrograde reaction textures. *Contributions to Mineralogy and Petrology*, **129**, 43–52.
- Thakur, V.C., 1973. Events in Alpine deformation and metamorphism in the northern Pennine Zone and southern Gottard Massif regions, Switzerland. *Geologische Rundschau*, **62**, 549–563.
- Tinkham, D.K., Zuluaga, C.A. & Stowell, H.H., 2001. Metapelite phase equilibria modeling in MnNCKFMASH: the effect of variable Al_2O_3 and $\text{MgO}/(\text{MgO} + \text{FeO})$ on mineral stability. *Geological Materials Research*, **3**, 1–42.
- Todd, C.S. & Engi, M., 1997. Metamorphic field gradients in the Central Alps. *Journal of Metamorphic Geology*, **15**, 513–530.
- Torres-Ruiz, J., Pesquera, A., Gil-Crespo, P.P. & Velilla, N., 2003. Origin and petrogenetic implications of tourmaline-rich rocks in the Sierra Nevada (Betic Cordillera, southeastern Spain). *Chemical Geology*, **197**, 55–86.
- Valley, J.W., Kitchen, N., Kohn, M.J., Niendorf, C.R. & Spicuzza, M.J., 1995. UWG-2, a garnet standard for oxygen isotope ratios: strategies for high precision and accuracy with laser heating. *Geochimica et Cosmochimica Acta*, **59**, 5223–5231.
- Vance, D. & O'Nions, R.K., 1992. Prograde and retrograde thermal histories from the central Swiss Alps. *Earth and Planetary Science Letters*, **114**, 113–129.
- Vielzeuf, D., Champenois, M., Valley, J.W., Brunet, F. & Devidal, J.L., 2005a. SIMS analyses of oxygen isotopes: matrix effects in Fe-Mg-Ca garnets. *Chemical Geology*, **223**, 208–226.
- Vielzeuf, D., Veschambre, M. & Brunet, F., 2005b. Oxygen isotope heterogeneities and diffusion profile in composite metamorphic-magmatic garnets from the Pyrenees. *American Mineralogist*, **90**, 463–472.
- Williams, M.L., 1994. Sigmoidal inclusion trails, punctuated fabric development, and interactions between metamorphism and deformation. *Journal of Metamorphic Geology*, **12**, 1–21.
- Williams, P.F. & Jiang, D., 1999. Rotating garnets. *Journal of Metamorphic Geology*, **17**, 367–378.
- Yang, P. & Rivers, T., 2001. Chromium and manganese zoning in pelitic garnet and kyanite: spiral, overprint, and oscillatory(?) zoning patterns and the role of growth rate. *Journal of Metamorphic Geology*, **19**, 455–474.
- Yang, P. & Rivers, T., 2002. The origin of Mn and Y annuli in garnet and the thermal dependence of P in garnet and Y in apatite in calc-pelite and pelite, Gagnon terrane, western Labrador. *Geological Materials Research*, **4**, 1–35.
- Yonkee, W.A., Parry, W.T. & Bruhn, R.L., 2003. Relations between progressive deformation and fluid-rock interaction during shear-zone growth in a basement-cored thrust sheet, Sevier orogenic belt, Utah. *American Journal of Science*, **303**, 1–59.
- Young, E.D. & Rumble, D., 1993. The origin of correlated variations in in-situ $^{18}\text{O}/^{16}\text{O}$ and elemental concentrations in metamorphic garnet from southeastern Vermont, USA. *Geochimica et Cosmochimica Acta*, **57**, 2585–2597.
- Zulauf, G. & Heflerich, S., 1997. Strain and strain rate in a synkinematic trondhjemite dike: evidence for melt-induced strain softening during shearing (Bohemian Massif, Czech Republic). *Journal of Structural Geology*, **19**, 639–652.

Received 8 March 2012; revision accepted 22 October 2012.